1 **TITLE Disordered clusters of Bak dimers rupture mitochondria during apoptosis**

2 **AUTHORS/AFFILIATIONS**

3 Rachel T. Uren[1,2], Martin O'Hely[1,2,3], Sweta Iyer[1,2], Ray Bartolo[1,4], Jason M. Brouwer[1,2], Amber E.
4 Alsop[1,2], Grant Dewson[1,2], Ruth M. Kluck*[1,2].

5 1. The Walter and Eliza Hall Institute of Medical Research, 1G Royal Parade, Parkville, Victoria,
6 3052, Australia

7 2. Department of Medical Biology, The University of Melbourne, 1G Royal Parade, Parkville,
8 Victoria, 3052, Australia

9 3. MOH Current address: Barwon Infant Study, Deakin University, PO Box 218, Geelong, Victoria,
10 3220, Australia

11 4. RB Current address: Murdoch Children's Research Institute, The Royal Children's Hospital,
12 Flemington Road, Parkville, Victoria, 3052, Australia

13 **CONTACT**

14 * Corresponding author Ruth M. Kluck, The Walter and Eliza Hall Institute of Medical Research,
15 1G Royal Parade, Parkville, Victoria, 3052, Australia, Tel: +61 3 9345 2487; Fax: +61 3 9347
16 0852; Email: kluck@wehi.edu.au

17

ABSTRACT

During apoptosis, Bak and Bax undergo major conformational change and form symmetric dimers that coalesce to perforate the mitochondrial outer membrane via an unknown mechanism. We have employed cysteine labelling and linkage analysis to the full length of Bak in mitochondria. This comprehensive survey showed that in each Bak dimer the N-termini are fully solvent-exposed and mobile, the core is highly structured, and the C-termini are flexible but restrained by their contact with the membrane. Dimer-dimer interactions were more labile than the BH3:groove interaction within dimers, suggesting there is no extensive protein interface between dimers. In addition, linkage in the mobile Bak N-terminus (V61C) specifically quantified association between dimers, allowing mathematical simulations of dimer arrangement. Together, our data show that Bak dimers form disordered, compact clusters to generate lipidic pores. These findings provide a molecular explanation for the observed structural heterogeneity of the apoptotic pore.

INTRODUCTION

The Bcl-2 family of proteins are the principal regulators of apoptotic cell death, with either Bak or Bax required to permeabilise the mitochondrial outer membrane (Lindsten et al., 2000, Wei et al., 2001). Bak and Bax are triggered to convert to their activated conformation by the binding of BH3-only relatives such as Bid and Bim (Gavathiotis et al., 2010, Dai et al., 2011, Du et al., 2011, Czabotar et al., 2013, Leshchiner et al., 2013, Brouwer et al., 2014), and once activated can be sequestered by pro-survival relatives such as Mcl-1 and Bcl-x_L (Llambi et al., 2011).

The ability of Bak and Bax to change conformation and oligomerize in the mitochondrial outer membrane appears crucial for their capacity to perforate this membrane (Westphal et al., 2014). Both proteins comprise nine α-helices that adopt a globular fold in the non-activated state (Suzuki et al., 2000, Moldoveanu et al., 2006). Non-activated Bak is anchored in the mitochondrial outer membrane via the α9-helix forming a transmembrane domain (Iyer et al., 2015). In contrast, non-

activated Bax is largely cytosolic due to binding of α9 to its own hydrophobic groove (Wolter et al., 1997, Gahl et al., 2014). Following binding of BH3-only proteins, both Bak and Bax undergo similar conformation changes including α1 dissociation (Weber et al., 2013, Alsop et al., 2015) and separation of the "latch" domain (α6-α8) (Czabotar et al., 2013, Brouwer et al., 2014) from the "core" domain (α2-α5). The core and α6 then collapse onto the membrane surface and become shallowly inserted into the membrane to lie in-plane (Aluvila, 2014, Bleicken et al., 2014, Westphal et al., 2014). Symmetric homodimers then form when the exposed BH3 domain of each molecule is re-buried in the hydrophobic groove of another activated molecule (Dewson et al., 2008, Dewson et al., 2012, Czabotar et al., 2013, Brouwer et al., 2014). Bax oligomers may also form prior to membrane insertion (Luo et al., 2014, Sung et al., 2015).

How symmetric homodimers of Bak or Bax then associate to porate the mitochondrial outer membrane is still unknown. Although there is structural information for Bak and Bax homodimers, no structures of higher order oligomers of Bak or Bax have been resolved. Bak and Bax have been shown to coalesce into clusters at the mitochondria upon an apoptotic stimulus (Nechushtan et al., 2001) and small clusters of Bax have been implicated in the rapid release of cytochrome *c* (Zhou and Chang, 2008). The availability of full-length recombinant Bax makes biochemical assays more amenable for Bax than for Bak. Thus, Bax complexes of various shapes and sizes have recently been detected with fluorescence microscopy of recombinant Bax on artificial membranes (Subburaj et al., 2015). Furthermore, super-resolution microscopy has shown Bax can be found in ring-like structures, arcs and clusters at the mitochondrial outer membrane of apoptotic cells (Grosse et al., 2016, Salvador-Gallego et al., 2016), although the orientation of Bax dimers in these structures could not be visualised. Higher order oligomers of both Bak and Bax vary in size when assessed by gel filtration, blue native PAGE or linkage (George et al., 2007, Dewson et al., 2012). Moreover, linkage studies have identified several points at which dimers might associate, including interactions at α-helices 1, 3, 5, 6, and 9 (Dewson et al., 2008, Dewson et al., 2009, Zhang et al., 2010, Pang et al., 2012, Ma et al., 2013, Aluvila, 2014, Bleicken et al., 2014, Gahl et al., 2014, Iyer

68 et al., 2015, Zhang et al., 2016). Critically, it is not clear whether any of these interaction sites are
69 required for dimer-dimer association and assembly of the apoptotic pore. Here, we compare
70 linkages through the full length of Bak in cells and show that dimers associate in a disordered, lipid-
71 mediated fashion.

72 **RESULTS**

73 ***The Bak N-segment, α1 and α1- α2 loop are solvent-exposed in Bak oligomers***

74 To resolve how Bak dimers coalesce to porate the mitochondrial outer membrane, we sought to
75 generate a more detailed biochemical map of the membrane topology of Bak dimers. This work
76 complemented our previous cysteine-accessibility analyses of Bak α5, α6 and α9 (Westphal et al.,
77 2014, Iyer et al., 2015), by analyzing the Bak N-terminus and additional residues in the α2-α5 core
78 and C-terminus. The two native cysteine residues of human Bak (C14 and C166) were first
79 substituted with serine to generate Bak Cys null (BakΔCys, i.e. C14S/C166S), and then a single
80 cysteine residue substituted at several positions throughout the molecule. Each Bak variant was
81 stably expressed in *Bak*$^{-/-}$*Bax*$^{-/-}$ mouse embryonic fibroblasts (MEFs) and tested for function (Figure
82 S1). To convert Bak to the activated oligomeric form, membrane fractions enriched for
83 mitochondria were incubated with tBid, as previously (Dewson et al., 2008). To label solvent-
84 exposed cysteine residues, membrane fractions were treated with the thiol-specific labelling reagent
85 IASD (4-acetamido-4'-((iodoacetyl) amino)stilbene-2,2'-disulfonic acid). Two negative sulfonate
86 charges prevent IASD from accessing cysteine in hydrophobic environments (such as the
87 mitochondrial outer membrane or the hydrophobic protein core), and also allow isoelectric focusing
88 (IEF) to resolve IASD-labelled and IASD-unlabelled Bak (Tran et al., 2013, Westphal et al., 2014).
89 We assessed each cysteine-substituted Bak variant for labelling before, during or after incubation
90 with recombinant tBid or tBid^{Bax}, a tBid variant containing the Bax BH3 domain (Hockings et al.,
91 2015), that activates Bak analogous to tBid, as well as a control not exposed to IASD and another
92 fully exposed to labelling by denaturation and membrane solubilization (Figure 1A, Figure S2). The

93 approach thus monitors solvent-exposure of the residue as non-activated Bak converts to oligomeric
94 Bak, and may detect transient exposure during these conformational changes.

95 In the N-terminus, most tested residues were accessible to IASD even before tBid treatment (Figure
96 1B and S2), consistent with the crystal structure (2IMT) (Moldoveanu et al., 2006). Two residues in
97 α1 (R36C and Y41C) that were not fully accessible before tBid treatment became exposed
98 following incubation with tBid (Figures 1B and S2). Two additional α1 residues, Q44C and Q47C,
99 also showed a tendancy for increased labelling. These changes suggest that the α1-α2 loop separates
100 from α1, consistent with increased labelling of A54C in the α1-α2 loop that opposes α1. Thus,
101 increased labelling of cysteine residues placed throughout the N-segment, α1 and the α1-α2 loop,
102 together with exposure of several N-terminal antibody epitopes (Alsop et al., 2015), indicate that
103 the Bak N-terminus becomes completely solvent-exposed after activation (Figure 1D).

104 To complete our survey of the core and C-termini of Bak dimers (Westphal et al., 2014, Iyer et al.,
105 2015), we tested the cysteine accessibility of additional selected residues in the α2-α5 core and the
106 α7-α8 region (Figures 1B and S2). A summary of current and previous cysteine labelling data for
107 the full length of the Bak protein in Figure 1C provides the following picture of Bak dimer
108 topology. Certain cysteine residues placed in α2 became transiently exposed, consistent with
109 exposure of the BH3 domain and then its burial in the hydrophobic groove in the α2-α5 core dimer
110 (Figure 1C), as predicted by the published structure of the Bak BH3:groove homodimer (4U2V)
111 (Brouwer et al., 2014). Cysteine substitutions on the exposed surface of α3 were successfully
112 labelled with IASD before, during and after tBid treatment. In contrast, two buried residues in α4
113 were refractory to IASD labelling throughout. In the α4-α5 linker region, although I123C became
114 more exposed following activation, it was still incompletely labelled. This may reflect loss of
115 contact between I123C and two hydrophobic residues in the "latch" (I167 and W170), followed by
116 shallow membrane insertion of I123C as it resides on the hydrophobic face of the Bak dimer core.
117 Partial labelling of this residue is consistent with shallow membrane insertion as IASD can label

118 cysteine moieties up to 7.5 Å into the hydrocarbon core of a lipid bilayer (Grundling et al., 2000,
119 Westphal et al., 2014). Within the C-termini, the profile of IASD-labelling was consistent with the
120 amphipathic α6 helix lying in-plane on the membrane surface (Westphal et al., 2014) and the
121 hydrophobic α9 forming the sole transmembrane domain (Figure 1D).

122 In summary, Bak undergoes a series of conformational changes as it transitions from its non-
123 activated monomeric state, to an activated BH3-exposed monomeric intermediate, to the symmetric
124 dimer that is the building block of the Bak oligomer (Figure 1D). In the course of these structural
125 rearrangements, some regions of Bak display changes in solvent exposure (such as α1 which
126 becomes more exposed, or α2 which is transiently exposed) whilst others remain buried throughout
127 (such as the α9 transmembrane anchor).

128 ***The N- and C-termini of activated Bak are mobile***

129 Linkage studies have provided significant insight into structural changes in Bak, as well as how the
130 activated proteins associate into high order oligomers (Dewson et al., 2008, Dewson et al., 2009,
131 Ma et al., 2013, Aluvila, 2014, Brouwer et al., 2014, Iyer et al., 2015). To directly compare reported
132 linkages, and to analyse the full length of Bak, we used our expanded library of single-cysteine Bak
133 variants. Each substituted cysteine was tested for the ability to disulphide bond to the same residue
134 in a neighbouring Bak molecule (or to a cysteine in a nearby protein) upon addition of the oxidant
135 copper phenanthroline (CuPhe). Linkage between Bak molecules was indicated by the presence of
136 2x complexes corresponding to twice the molecular weight of the Bak monomer on non-reducing
137 SDS-PAGE. It is important to note that these 2x complexes are the product of CuPhe-mediated
138 linkage between Bak molecules and do not necessarily represent the native Bak BH3:groove dimer
139 that will form even in the absence of linkage, as shown below on BNP. This system of single
140 cysteine substitutions offers an elegant screening approach for assessing the proximity of single
141 cysteine residues in neighbouring molecules in a point-to-point manner, but does not identify

142 interaction surfaces where a single cysteine substitution may not contact its counterpart (See
143 Discussion).

144 Even in the absence of tBid treatment, cysteine residues in flexible regions displayed some linkage
145 to neighbouring non-activated Bak molecules (Figure 2, upper panels). For example, some 2x
146 complexes were captured by cysteine substitutions in the flexible N-segment (G4C, C14, L19C,
147 S23C), and α1-α2 loop (G51C, D57C, P58C, Q66C, S68C, S69C), indicating some proximity of
148 Bak monomers in untreated mitochondria. Furthermore, disulphide linkage to proteins other than
149 Bak resulted in Bak complexes larger than the 2x species and was observed for cysteine
150 substitutions in the α2-α3 helices (D84C, R87C), α4-α5 loop (S121C, N124C), α8-α9 linker
151 (G186C, I188C) and C-terminal end of α9 (V205C). This is unsurprising as the MOM is a protein-
152 rich environment and there are documented examples of monomeric Bak associating with other
153 membrane proteins such as VDAC2 (Cheng et al., 2003, Lazarou et al., 2010, Ma et al., 2014).

154 After addition of tBid had activated Bak, each cysteine in the N-extremity (a region comprising the
155 N-terminus, α1 and α1-α2 loop) showed more efficient linkage to 2x complexes (Figure 2A, upper
156 panel). The freedom with which each cysteine in the N-extremity of Bak can link suggests this
157 region is highly mobile and does not engage in stable protein-protein or protein-lipid interactions
158 following activation. In contrast, cysteine residues positioned in the core (α2-α5) showed relatively
159 modest linkage to 2x complexes (Figure 2B, upper panel), consistent with lack of flexibility in the
160 α2-α5 core dimer (Brouwer et al., 2014) and its relative immobility due to association with the
161 membrane.

162 We next addressed linkage in the C-extremity encompassing the α6-α8 latch and α9 transmembrane
163 domain (Figure 2C, upper panel). After Bak activation, H164C in α6 showed increased linkage to
164 2x complexes, as reported previously (Dewson et al., 2009, Ma et al., 2013). Cysteine substitutions
165 in the α8-α9 loop and the beginning of the α9 transmembrane domain (up to residue N190C) also
166 showed linkage to 2x complexes (Figure 2C, upper panel). However, compared to the N-extremity,

167 linkage was less complete, possibly due to membrane association limiting mobility. Linkage of
168 membrane-buried α9 residues was even less efficient (Figure 2C). However, at a higher temperature
169 α9 residues show much stronger linkage (Figure S3) (Iyer et al., 2015), attributable to increased Bak
170 mobility or CuPhe penetration into the bilayer.

171 In summary, after Bak activation, the whole N-extremity is highly dynamic due to being fully
172 solvent-exposed; the core is constrained and membrane-associated; and the C-extremity is flexible,
173 but is anchored to the membrane.

174 ***Mobility of the N- and C-extremities permits linkage between dimers***

175 We next used blue native PAGE (BNP) to consider two types of cysteine-mediated Bak linkage:
176 linkage *within* Bak dimers and linkage *between* Bak dimers. The Bak BH3:groove interaction
177 *within* dimers is an extensive protein-protein interface and is stable in 1% digitonin on BNP while
178 the interaction between dimers is not (Ma et al., 2013). Thus oligomerized Bak migrates only as
179 BH3:groove dimers on BNP. Addition of CuPhe to mitochondrial extracts prior to BNP can
180 stabilise high order complexes on BNP and does so by cysteine-mediated linkage *between* dimers
181 (Ma et al., 2013). Thus, if addition of CuPhe at the end of the mitochondrial incubation generated
182 4x and greater complexes on BNP, we conclude that the linkage was *between* dimers. If larger
183 complexes were absent and dimers predominated on BNP, any linkage was *within* the dimer. Thus,
184 parallel examination of CuPhe linked Bak species on BNP and non-reducing SDS PAGE permits
185 differentiation of three conditions: linkage *within* the dimer, linkage *between* dimers, or no cysteine
186 linkage (Figure 3A).

187 In the N-extremity (G4C to S69C), each introduced cysteine could link some dimers to larger
188 complexes on BNP (Figure 2A, lower panel). Upon tBid activation, SDS-PAGE showed an
189 increased proportion of 2x complexes, and higher order complexes (>10x) were observed on BNP
190 for all residues. Of note was a stretch of residues from E59 to T62 that, following tBid treatment,

191 exhibited very efficient linkage by SDS-PAGE (obvious 2x, negligible 1x). In this stretch, BNP
192 showed no dimer species and a concomitant shift to 4x species and higher order complexes,
193 indicating efficient linkage between dimers but no linkage within dimers. Residues closer to the α2-
194 α5 core (Q66C to S69C), showed progressively more 1x species (SDS-PAGE) and an increase in
195 dimers (BNP), indicative of becoming closer to the constrained core of the dimer. Together, these
196 linkage data further argue that dimers possess flexible N-extremities capable of efficient linkage
197 within and between dimers, with linkage becoming exclusively between dimers as residues
198 approach the constrained α2-α5 core (Figure 3B). Interestingly, because linkage of cysteine residues
199 in the E59-T62 region occurs *only* between dimers, and is very efficient, this linkage provides a
200 molecular sensor that can specifically quantitate dimer-dimer interactions, and is the first assay to
201 do so.

202 In the Bak C-terminus also, cysteines could link dimers to larger complexes on BNP, although a
203 striking laddering pattern was apparent (Figure 2C, lower panels). For example, the large (>10x)
204 complexes common at the highly mobile N-extremity were not apparent at the membrane-
205 associated C-extremity. Stronger ladders for certain residues may be explained by the membrane
206 associated α6-α8 allowing only certain residues to be presented laterally. Lastly, linkage in the C-
207 extremity may be only between dimers (rather than within dimers) as the proportion of 2x to 1x
208 species on SDS-PAGE is similar to the proportion of high order complexes to dimers on BNP.

209 ***Single-cysteine mutants in the rigid core capture some linkage, mostly at the lateral edges***

210 Previous studies suggested that the structured α2-α5 core of the Bak (or Bax) dimer might form a
211 dominant, symmetric interface capable of driving dimers to form higher order complexes (Aluvila,
212 2014, Brouwer et al., 2014). For example, crystals of the Bak α2-α5 core dimer showed a side-by-
213 side association (4U2V)(Brouwer et al., 2014). However, this was attributed to crystal packing
214 effects, as chemical crosslinking between the α4-α5 loops was not detected (Brouwer et al., 2014).
215 Accordingly, in the present studies, disulphide bonding between the α4-α5 loops was not captured

216 with CuPhe (Figure 2B, lower). End-to-end associations were suggested by α3:α3' or α5:α5'
217 linkages (Aluvila, 2014, Brouwer et al., 2014), and disulphide bonding at the equivalent residues
218 was also evident in this study (H99C:H99C for α3:α3'; H145C:H145C' for α5:α5')(Figure 2B,
219 lower). Notably, this linkage was not as efficient as linkage observed for the N-extremity, and these
220 and other linkage-competent residues locate mostly to the lateral edges of the α2-α5 core dimer
221 when lying in-plane (Figure 3C). Thus, screening individual cysteine substitutions in the Bak dimer
222 core for linkage did not uncover any dominant sites of interaction between Bak dimers, but showed
223 widespread linkage of residues around the lateral edges of the dimer, consistent with the random
224 collision of Bak dimers.

225 These findings support a flexible extremity model for full-length Bak dimers in the MOM, outlined
226 in Figure 3D with side-on (left) and top-down views (right). At the centre is the α2-α5 core dimer
227 lying in-plane and partially submerged in the membrane surface. Extending from both sides of the
228 core dimer is a flexible latch (α6-α8) of ~50 residues that also lies in-plane and connects to the
229 transmembrane α9-helices. Extending from both ends of the dimer core is the solvent-exposed,
230 flexible and mobile N-extremity of ~70 residues. Each circle in Figure 3D illustrates the range of
231 possible positions for the flexible N- and C-extremities (blue and pink respectively). Overlap of the
232 largest blue circles (labelled G4C) indicates the potential for residues close to the N-terminus to link
233 within dimers. In contrast, the smaller blue circles (labelled V61C) do not overlap, indicating a lack
234 of linkage within the dimer at this residue. Notably, these linkage constraints are consistent with the
235 dimensions of the α2-α5 dimer core as determined from the recent crystal structure (4U2V) (Figure
236 3E).

237 These findings also reveal how dimers associate into high order oligomers. As linkage can be
238 induced between several regions of the Bak dimer, there is no dominant protein-protein interface
239 that mediates dimer assembly into high order oligomers. Rather, the linkage pattern is consistent
240 with transient collision of dimers in-plane on the membrane. Collisions of the α2-α5 core and α6-α8

241 latch are limited by their membrane-association, whereas the flexible, entirely solvent-exposed N-
242 terminal region is free to link between dimers and does so very efficiently.

243 ***Inter-dimer interfaces are more labile to detergent than the intra-dimer (BH3:groove) interface***

244 We next examined if the inter-dimer interactions identified above were stable in digitonin, as shown
245 for the BH3:groove interface within dimers (Ma et al., 2013). Digitonin was added to the
246 mitochondrial incubations after Bak had become oligomerized by incubation with tBid, but prior to
247 disulphide bond formation induced by CuPhe (Figure 4A). As expected, digitonin did not prevent
248 linkage *within* dimers as shown by 2x complexes of M71C/K113C on SDS-PAGE (Figure 4A,
249 upper panel, lane 3). However, digitonin prevented all linkage *between* dimers on BNP of seven
250 single-cysteine variants (Figure 4A, lower panel), indicating that inter-dimer interactions are
251 mediated either by membrane or by weak protein-protein interactions.

252 These experiments also provided new insight into linkage within dimers. For example, two residues
253 at the far N- and C-termini (L19C and the C-terminal extension GGSGGCK (Iyer et al., 2015))
254 could link within dimers to generate 2x complexes on SDS-PAGE after digitonin treatment (Figure
255 4A, upper panel). Thus, these residues were sufficiently distal from the core to reach their
256 counterpart across the length of the structured α2-α5 core dimer and allow linkage within the dimer
257 (Figure 3D, 3E). On BNP, dimers of these two residues (L19C, and to a lesser extent GGSGGCK)
258 also migrated faster than dimers of other variants (Figure 4A, lower panel), suggesting that linkage
259 within the dimer caused a more compact, faster migrating protein complex under these native
260 conditions.

261 ***Bak dimers can become interspersed by Bax***

262 To test if interactions between Bak dimers could be disrupted by other proteins, and thus test if Bak
263 dimer aggregation was a dynamic, reversible process, we added recombinant proteins from the Bcl-
264 2 protein family after Bak had formed dimers (Figure 4B). Dimer interactions were monitored by

265 linkage between the N-termini (V61C:V61C') or C-termini (H164C:H164C'), and compared to
266 BH3:groove linkage (M71C:K113C). To oligomerize Bak, mitochondria were first incubated with
267 $tBid^{M97A}$, a variant that binds poorly to prosurvival proteins such as Bcl-x_L and Mcl-1 (Lee et al.,
268 2016). Mitochondria were then incubated with recombinant Bax, Bcl-x_L or Mcl-1ΔNΔC. Finally,
269 CuPhe was applied and the extent of disulphide linkage assessed by non-reducing SDS-PAGE
270 (Figure 4B). Notably, Bax translocated to mitochondria and decreased linkage between Bak dimers
271 (e.g. V61C:V61C' and of H164C:H164C') but not within dimers (e.g. M71C:K113C) (Figure 4B).
272 In contrast, recombinant Bcl-x_L and Mcl-1ΔNΔC translocated to the mitochondrial membrane but
273 did not interfere with linkage between Bak dimers (Figure 4B). Thus, Bax not only localised to the
274 same membrane microdomain as the pre-formed Bak oligomers, but became partially interspersed
275 with the dimers, indicating that dimer aggregation is dynamic.

276 ***V61C:V61C' linkage can monitor dimer-dimer interactions; stochastic simulations reveal a***
277 ***disordered aggregate of Bak dimers***

278 Our biochemical data support the random collision of Bak dimers at the mitochondrial outer
279 membrane during apoptosis. Indeed, several studies indicate that Bax and Bak can reside in a
280 variety of different structures at the mitochondrial outer membrane of apoptotic cells, including
281 clusters (Nechushtan et al., 2001, Zhou and Chang, 2008, Grosse et al., 2016, Nasu et al., 2016,
282 Salvador-Gallego et al., 2016). To test if random collisions between dimers could feasibly explain
283 the linkage patterns observed, simulations of the random contact between dimers were performed.
284 The efficient and exclusive linkage that occurs between dimers at residue V61C formed the basis of
285 our simulations (Figure 5).

286 To simulate the aggregation of Bak dimers on the mitochondrial outer membrane, this complex
287 biological system was simplified to limit the number of parameters required to mimic the
288 experimental outcome. We simulated the membrane as a flat surface (i.e. a 2D plane). Each subunit
289 representing a Bak dimer, was evenly distributed on a geometric grid imposed on this surface

290 (Figure 6A), and to avoid edge effects the grid was wrapped onto a torus. A hexagonal grid, rather
291 than square or triangular, was selected to best represent the close packing of objects on a plane with
292 the greatest degrees of freedom. The linkage potential of each subunit in the grid was based on the
293 known linkage constraints of the V61C residue; i.e. linkage occurred exclusively and efficiently
294 between dimers and each dimer could make at most 2 cysteine linkages, but possibly only 1 or 0
295 linkages if no other free cysteines were available. Furthermore, the simulation allowed linkages
296 only between immediately adjacent dimers, based on the short 4 Å limit of the CuPhe-mediated
297 disulphide linkage and the known dimensions of the Bak dimer. Thus, each hexagonal subunit had
298 the freedom to link with at most two neighbouring hexagons, in any direction, and this random
299 linkage between neighbouring dimers would result in a mixture of linkage states including double,
300 single or no linkages. With this hexagonal grid, four types of double linkage were possible;
301 opposite, obtuse, acute or reciprocal (Figure 6B). An equal probability for each of the double
302 linkages (opposite, obtuse, acute or reciprocal) was imposed, to reflect close but random packing of
303 dimers at the membrane. Furthermore, the simulation was allowed to proceed to complete linkage
304 of available cysteine residues, to reflect the near-complete linkage of V61C:V61C'. With these few
305 parameters, a complex biological system was elegantly reduced to a simplified simulation.

306 The simulation output was a frequency distribution of the number of Bak dimers present in each
307 linked complex (Figure S4). To approximate the BNP western blot densitometry, the counts were
308 then multiplied by the number of Bak dimer units (e.g. 1, 2, 3, 4 etc) in each of the linked Bak
309 complexes, and the predicted densitometry smoothed with a gaussian kernel to allow qualitative
310 comparison with the gaussian-like densitometry output from the BNP western blots.

311 Notably, the simulation produced outputs that closely matched the distinctive linkage pattern
312 observed for V61C, i.e. prominent 4x complexes and complexes greater than 10x the Bak molecular
313 weight (compare Figure 5A, 5B with Figure 6C, 6D). Thus, the simulations provided proof of
314 principle that the linkage pattern (V61C:V61C') observed in mitochondria can be explained by

315 random dimer arrangement. These logic arguments based on the linkage constraints of the V61C
316 residue have, for the first time, afforded single molecule resolution of Bak aggregation.

317 ***Simulations are robust to a reduction in linkage***

318 To explore robustness of the simulations, we asked if the simulation could predict the linkage
319 pattern when linkage was limited due either to less V61C residues, or to cysteine residues at
320 positions other than V61C. In the first test, we performed mitochondrial experiments in which
321 ~50% of the Bak molecules lacked cysteine residues. In those experiments, Bak V61C was co-
322 expressed with Bak Cys-null that was FLAG-tagged (Figure S5A, upper panel). As expected, only
323 half of the Bak molecules could link to 2x species after activation by tBid and induction of linkage
324 (Figure S5A, middle panel, lane 4). In addition, all molecules formed BH3:groove dimers after
325 incubation with tBid, as shown by BNP, but the capture of higher order oligomers mediated by
326 cysteine-linkage was greatly reduced (Figure S5A, lower panel, lane 4; quantified in Figure S5B).
327 In simulations of this system, we assumed equal expression of V61C and the Cys null variants, as
328 indicated by western blot analysis. We also assumed that this population of monomers forms dimers
329 in Mendelian proportions: 25% of dimers are V61C doublets and can link twice, 50% are
330 V61C:Cys null and can link once, and the remaining 25% are Cys null doublets and cannot link
331 (Figure S5C). The simulation output (Figure S5D) reflected that of the BNP densitometry (Figure
332 S5B) in terms of more dimers and fewer >10x complexes, indicating the simulation was
333 generalizable to a different distribution of linkage-competent Bak molecules.

334 We next examined if our simulations were also robust when approximating the linkage pattern of
335 residues other than V61C (Figure S6A). As noted above, because T62C, Q66C, S68C, and S69C
336 substitutions were closer than V61C to the constrained α2-α5 core, they did not link efficiently
337 (Figure 2A lower, quantified in Figure S6B). To simulate this steric hindrance caused by a shorter
338 distance from the constrained core, an *edge blocking* effect was introduced to the model; every edge
339 of every hexagon was prohibited from having a link form across it with this probability for the

340 duration of each simulation. As the edge blocking probability increased from 0 to 0.75, linkage
341 between dimers decreased to generate patterns comparable to BNP analysis of these core-proximal
342 residues (Figure S6C). Thus, modification of a single parameter could describe linkage of residues
343 closer than V61C to the Bak dimer core. The adaptability of this simple simulation further
344 illustrated the strength and feasibility of our model of random Bak dimer aggregation at the
345 mitochondrial outer membrane during apoptosis.

346 **DISCUSSION**

347 Here we investigated the topology of Bak dimers in the mitochondrial outer membrane, and how
348 dimers assemble into the high order oligomers thought necessary to form apoptotic pores in that
349 membrane. We found that Bak dimers are characterized by flexible N- and C-extremities flanking a
350 rigid α2-α5 core, and that these dimers aggregate in disordered, dynamic, compact clusters.
351 Critically, we found no evidence for a single, dominant protein-protein interface between dimers
352 and predict the lipid environment plays a crucial role in facilitating the aggregation of dimers and
353 subsequent membrane rupture.

354 We had previously proposed the in-plane model for Bak dimers (Westphal et al., 2014). Our current
355 data advances this model to show the N- and C-extremities are flexible, based on analysis of the
356 full-length of Bak when activated and dimerised at the mitochondrial outer membrane (Figure 3D).
357 The N-extremity (~70 residues C-terminal to α2) becomes fully solvent-exposed as shown by IASD
358 labelling, and fully mobile as indicated by linkage, consistent with exposure of N-terminal cleavage
359 sites and antibody epitopes in α1 and the α1-α2 loop (Griffiths et al., 1999, Weber et al., 2013,
360 Alsop et al., 2015). Failure of the N-extremity to re-engage in protein-protein or protein-lipid
361 interactions argues that it does not contribute to the assembly of dimers. The remainder of Bak is
362 membrane-associated, with the α2-α5 core and α6 (and possibly α7-α8) in-plane with the outer
363 mitochondrial membrane surface and partially embedded (Aluvila, 2014, Brouwer et al., 2014,
364 Westphal et al., 2014) while α9 forms a transmembrane domain (Iyer et al., 2015). The topology of

365 the α2-α5 region is consistent with the α2-α5 core dimer crystal structure (~35Å × 45Å)(Brouwer et
366 al., 2014), as V61C (~30Å from the core dimer) linked between dimers but not within dimers.
367 Flexibility of the C-terminal α6-α9 region, as indicated by multiple linkages between these regions
368 (Bleicken et al., 2014, Iyer et al., 2015, Zhang et al., 2016), implies that embedded dimers adopt a
369 range of conformations on the MOM surface (Figure 7A).

370 Linkage experiments have identified several possible interactions between dimers of Bak or Bax
371 (Dewson et al., 2008, Dewson et al., 2009, Zhang et al., 2010, Pang et al., 2012, Ma et al., 2013,
372 Aluvila, 2014, Bleicken et al., 2014, Gahl et al., 2014, Iyer et al., 2015, Zhang et al., 2016), with
373 many also shown in the present study. Notably, however, a dominant protein-protein interface
374 between dimers was not evident. Rather, linkage between the membrane-associated regions could
375 be detected at many positions, arguing for a disordered arrangement. As our single-cysteine
376 scanning approach can only examine the homotypic pairing of cysteine residues, it remains possible
377 that heterotypic pairing of cysteine substitutions may detect a more complex protein interface
378 between dimers, as seen for near complete linkage at the Bak BH3:groove interface (M71C:K113C,
379 Figure 4B) (Dewson et al., 2008). However, in support of the notion that there is no dominant
380 protein interface between dimers, the interaction between Bak dimers is lost when digitonin is
381 added, in contrast to the BH3:groove interface which persists in the presence of digitonin.
382 Moreover, lability of dimer-dimer association was highlighted by the capacity of Bax to intermingle
383 with pre-formed Bak dimers. Each of Bcl_{xL}, Mcl-1 and Bax localised to mitochondria with similar
384 efficiency, however a critical feature of Bax is that, like Bak, following activation by tBid it
385 collapses onto the membrane surface to form homodimers (Westphal et al., 2014). The large
386 membrane surface occupied by Bax dimers, together with disturbance of the outer leaflet, may
387 explain why Bax, but not the prosurvival proteins, could disrupt Bak dimer-dimer association in this
388 assay.

389 A variety of biophysical and imaging techniques have been deployed to better understand how Bak
390 (or Bax) dimers associate, yet it remains unclear. Well-characterised pore-forming proteins
391 typically reveal an extensive interface between subunits that facilitates pore formation (Song et al.,
392 1996, Mueller et al., 2009). Versions of this regular architecture have recently been considered for
393 Bak and Bax as a closed circuit of dimers lining a circular pore (Aluvila, 2014, Bleicken et al.,
394 2014, Brouwer et al., 2014). In contrast to these hypothetical linear dimer arrangements, our
395 biochemical data revealed that there is no single dominant interface between the α2-α5 core dimers
396 and support the random collision of Bak dimers in two dimensions at the mitochondrial outer
397 membrane during apoptosis. Here a novel approach of mathematical modelling was used to
398 simulate linkage between Bak dimers and showed the feasibility of random dimer association. For
399 example, as the V61C residue linked only between Bak dimers, and did so very efficiently, this
400 provided a powerful tool for testing different arrangements of Bak dimers on the membrane. A
401 minimalist set of assumptions were adopted for stochastic simulations of V61C:V61C' linkage
402 between Bak dimers: linkage is complete and irreversible but occurs only between dimers; only two
403 linkages are possible per dimer; and neighbouring dimers can only link if both have a free cysteine
404 available for disulphide bonding. Indeed, the simulation showed good concordance with different
405 sets of linkage data obtained from fully oligomerised Bak in mitochondria. From this we conclude
406 that Bak dimers are closely packed and aggregate with a random orientation. As pores no longer
407 form if Bak levels decrease by ~50% in these cells (Ferrer et al., 2012), our observations from this
408 whole population of Bak represent the species of Bak dimers that contribute to pore formation,
409 rather than a minor species not involved in pore formation.

410 A disordered cluster of dimers is reminiscent of the "carpet" model of pore formation by peptides
411 (reviewed by (Gilbert, 2016)). Amphipathic antimicrobial peptides such as melittin lie parallel to
412 the membrane plane, with accumulation causing strain in the outer layer of the membrane until at
413 higher concentrations the lamellar structure of the membrane is destabilised and non-lamellar
414 lipidic pores are formed (Lee et al., 2008, Lee et al., 2013). Like an amphipathic peptide, the Bak

415 and Bax α2-α5 core dimers and α6-helices penetrate the outer leaflet of the bilayer (Czabotar et al.,
416 2013, Aluvila, 2014, Brouwer et al., 2014, Westphal et al., 2014). While very high concentrations
417 of antimicrobial peptides can disintegrate membrane in a detergent-like manner, this does not
418 appear to occur with near- physiological levels of Bak and Bax (Lee et al., 2008). Antimicrobial
419 peptides also have membrane thinning attributes (Chen et al., 2003), as reported for Bax (Satsoura
420 et al., 2012). Satsoura and colleagues discuss how membrane deformation by Bax may promote
421 oligomerization mediated not by protein:protein interactions but by long-range changes in
422 membrane tension (Satsoura et al., 2012). Thus, as illustrated in Figure 7B, we hypothesize that Bak
423 dimers penetrate the outer leaflet to attract further dimers and in doing so increase the membrane
424 disturbance. Enlarging clusters then destabilize the membrane sufficiently to form lipidic pores that
425 release apoptogenic factors. The pores may then be stabilized by parts of the Bak and Bax dimers
426 rearranging to line the pore and form proteolipidic pores (Terrones et al., 2004, Garcia-Saez, 2012,
427 Westphal et al., 2014). Hence, our model for the disordered clustering of Bak dimers provides a
428 holistic molecular explanation for the detection of Bak and Bax in a variety of formations including
429 complete rings, arcs, lines and random clusters (Grosse et al., 2016, Nasu et al., 2016, Salvador-
430 Gallego et al., 2016).

431 In conclusion, this study proposes a novel means of oligomerization by Bak and Bax in apoptotic
432 cells: that dimers aggregate in dense clusters without a dominant interface and this dynamic
433 association requires the involvement of the lipid membrane. We have described molecular tools that
434 can precisely monitor the aggregation of Bak dimers in cells, and could also be used to examine
435 how the pro-survival proteins inhibit Bak oligomerisation, which may impact on the development
436 of cancer therapies that target these proteins. Critically, the combination of linkage data and
437 mathematical simulations described here has offered, for the first time, insight into assembly of the
438 apoptotic pore with single molecule resolution.

439

440 **MATERIALS AND METHODS**

441 **Recombinant proteins**

442 Recombinant proteins were prepared as previously described; caspase 8-cleaved human Bid (tBid)
443 (as per (Kluck et al., 1999)), $tBid^{Bax}$ and Bcl-x_L full length (as per (Hockings et al., 2015)), Cys null
444 Bax full length (as per (Czabotar et al., 2013)), Mcl-1ΔN151ΔC23 (as per (Chen et al., 2005).
445 $tBid^{M97A}$ was kindly provided by E. Lee (Lee et al., 2016).

446 **Bak variant library cloning and expression**

447 A library of human Bak mutants was generated by site-directed cysteine substitution (as per
448 (Dewson et al., 2008). Human Bak with the endogenous cysteine residues mutated to serine (Bak
449 Cys null C14S/C166S) was used as the template in overlap extension PCR to introduce single
450 cysteine residues throughout the Bak sequence, and then cloned into the pMX-IRES-GFP retroviral
451 vector (primer and vector sequences available on request). Mutants were introduced into SV40-
452 immortalized *Bak*$^{-/-}$*Bax*$^{-/-}$ mouse embryonic fibroblasts (MEFs) by retroviral infection (as per
453 (Dewson et al., 2008).

454 **Preparation of membrane fractions enriched for mitochondria**

455 *Bak*$^{-/-}$*Bax*$^{-/-}$ MEFs expressing Bak cysteine mutants were permeabilised and membrane fractions
456 containing the mitochondria were isolated as previously described (Dewson et al., 2008). Cells were
457 washed in PBS and then re-suspended at a concentration of 1×10^7 cells/ml in wash buffer
458 supplemented with digitonin (100 mM sucrose, 20 mM HEPES-NaOH pH 7.5, 100 mM KCl, 2.5
459 mM $MgCl_2$, 4 μg/ml Pepstatin A (Sigma-Aldrich, St. Louis, MO, USA), Complete protease
460 inhibitors (Roche, Castle Hill, NSW, Australia) and 0.025% w/v digitonin (Calbiochem, Merck,
461 Darmstadt, Germany). Cells were incubated for 10 min on ice, then membrane fractions were
462 collected by centrifugation at 16,000 ×*g* for 5 min and the supernatant discarded. Pellets were re-

463 suspended in wash buffer (no digitonin), and permeabilisation of the cell membrane confirmed by
464 trypan blue uptake.

465 **Activation of Bak by tBid or Etoposide**

466 To assess the apoptotic function of each Bak variant in cells, *Bak*$^{-/-}$*Bax*$^{-/-}$ MEFs expressing Bak
467 cysteine mutants were treated with etoposide (10 μM) for 24 h, and cell death, as indicated by
468 propidium iodide (5 μg/ml) uptake, determined by flow cytometry (FACSCalibur, BD Biosciences,
469 San Jose, CA, USA). To activate Bak and induce mitochondrial outer membrane permeabilisation
470 *in vitro*, membrane fractions from *Bak*$^{-/-}$*Bax*$^{-/-}$ MEFs expressing Bak cysteine variants were treated
471 with 100 nM recombinant tBid for 30 min at 30°C (as described in (Dewson et al., 2008). Selected
472 samples were treated with the functionally equivalent protein tBid^{Bax} in which the BH3 domain of
473 Bid was substituted with the Bax BH3 domain (Hockings et al., 2015).

474 **Cysteine accessibility to IASD labelling, one-dimensional isoelectric focussing and IASD**
475 **quantification**

476 The cysteine residue of each Bak variant was assessed for solvent exposure by incubating
477 membrane fractions with the cysteine-labelling reagent IASD (Molecular Probes® Life
478 Technologies, Carlsbad, CA, USA) for 30 min at 30°C (as described in (Westphal et al., 2014)).
479 Membrane fractions were supplemented with 100 μM TCEP to prevent oxidization of cysteines that
480 would inhibit IASD labelling. Samples were unlabelled, or incubated with IASD before, during or
481 after tBid incubation or following denaturation with 1% w/v ASB-16 (Merck). IASD labelling was
482 quenched by the addition of 200 mM DTT and samples solubilised in 1% ASB-16 for 10 min at
483 22°C. Soluble supernatant fractions were isolated by centrifugation at 16,000 ×*g* for 5 min, and
484 added to an equal volume of IEF sample buffer (7 M urea, 2 M thiourea, 2% w/v CHAPS,
485 Complete protease inhibitors, 4 μg/ml pepstatin A, 1% w/v ASB-16 and 0.04% w/v bromophenol
486 blue). Samples were loaded onto 12-well Novex® pH 3-7 IEF gels (Life Technologies) and focused

487 with a Consort EV265 power supply with increasing voltage (100 V for 1 h, 200 V for 1 h and 500
488 V for 30 min). IEF gels were pre-soaked in SDS buffer (75 mM Tris/HCl, pH 6.8, 0.6% w/v SDS,
489 15% v/v glycerol), and then transferred to PVDF membrane for western blot analysis.

490 IASD labelling was quantified (ImageLab 4.1, Bio-RAD) from western blots by measuring signal
491 intensity for the unlabelled and labelled Bak band species in each lane to calculate the percentage of
492 the total signal from each lane attributed to the faster migrating IASD-labelled species. A global
493 background subtraction was applied to regions of interest from each western blot. Data were
494 presented as the mean ± SD (n≥3), or range (n=2) and the number of replicates indicated on the *x*-
495 axis. A two-tailed unpaired t-test was employed to determine significant differences ($p<0.05$) in the
496 percentage of IASD labelled Bak before versus after tBid treatment.

497 **Oxidant-induced disulphide linkage (CuPhe)**

498 The cysteine residue of each Bak variant was tested for disulphide linkage with proximal cysteine
499 residues on Bak (or other proteins) by incubation with the oxidant copper phenanthroline (CuPhe)
500 (as per (Dewson et al., 2008)). CuPhe was prepared as a stock solution of 30 mM $CuSO_4$ and 100
501 mM 1,10-phenanthroline in 4:1 water/ethanol. Following incubation of membrane fractions with
502 tBid at 30 ^{o}C, samples were pre-chilled on ice for 5 min, and then incubated with a 100-fold
503 dilution of the CuPhe solution on ice for 15 min. Note that (Iyer et al., 2015) performed CuPhe
504 linkage without the pre-chill incubation. Disulphide bond formation (linkage) was quenched by the
505 addition of 20 mM N-ethyl maleimide (NEM, to label any remaining free cysteines, 10 min on ice)
506 and 5 mM EDTA (to chelate copper, 5 min on ice) and samples analysed by non-reducing SDS
507 PAGE or blue native PAGE (BNP).

508 **SDS PAGE and Blue Native PAGE**

509 CuPhe-linked samples were analysed by SDS PAGE (12% TGX gels (Life Technologies)) in the
510 absence of reducing agents to preserve disulphide bonds. The efficiency of linkage between Bak

511 molecules was measured by a shift in Bak migration from 1x to 2x complexes. To discriminate
512 between linkages occurring within or between Bak dimers, CuPhe-linked samples were also
513 analysed in tandem by blue native PAGE (BNP) to preserve the native dimer interface (i.e. the
514 BH3:groove interface) in addition to any disulphide bonds between Bak molecules. Migration of
515 higher order linked complexes (i.e. greater than dimer) on BNP indicated the presence of disulphide
516 bonds between Bak dimers. Following quenching of CuPhe with NEM and EDTA, membrane
517 fractions were isolated by centrifugation at 16,000 ×*g* for 5 min. Supernatants were discarded and
518 membrane pellets were solubilised in 20 mM Bis-Tris pH 7.4, 50 mM NaCl, 10% v/v glycerol, 1%
519 w/v digitonin, and incubated on ice for 1 h and insoluble material was removed by centrifugation at
520 16,000 ×*g* for 5 min. The resulting supernatants were prepared for BNP by the addition of Native
521 Sample buffer (Life Technologies) and Coomassie Additive (Life Technologies), and then loaded
522 onto Novex® 4-16% Native PAGE 1.0 mm 10 well gels as per the manufacturer's instructions (Life
523 Technologies). Western blot transfer to PVDF was performed at 30 V for 150 min in transfer buffer
524 (25 mM Tris, 192 mM Glycine, 20% v/v Methanol) supplemented with 0.037 % w/v SDS. PVDF
525 membranes were de-stained with 10% v/v acetic acid 30% v/v ethanol, then further de-stained in
526 methanol and rinsed thoroughly with dH_2O before immunoblotting.

527 **Immunoblotting**

528 SDS PAGE and IEF membranes were immunoblotted for Bak using the rabbit polyclonal anti-Bak
529 aa23-38 (B5897, Sigma-Aldrich, Castle Hill, NSW, Australia). BNP membranes were
530 immunoblotted for Bak using an in-house anti-Bak monoclonal rat IgG (clone 7D10, WEHI,
531 (Dewson et al., 2009, Alsop et al., 2015)), except in the case of Bak mutants ranging from G51C to
532 P58C that were detected on BNP with the anti-Bak aa23-38. In-house monoclonal rat antibodies
533 were used to detect recombinant Bax (clone 49-F9, WEHI), Bcl-x_L (clone 9C9, WEHI) and Mcl-1
534 (clone 19C 4-15, WEHI). Horseradish peroxidase conjugated IgG secondary antibodies were used;
535 anti-rabbit (4010-05, Southern Biotech) and anti-rat (3010-05, Southern Biotech). Immobilised

536 horseradish peroxidase was detected with Luminata Forte western HRP substrate (WBLUF0500,
537 Millipore, Billerica, MA, USA), images captured with the ChemiDoc XRS+ System (Bio-RAD,
538 Hercules, CA, USA) and signal intensity measured with Image Lab 4.1 software (Bio-RAD).

539 **Blue Native PAGE densitometry**

540 Images were transformed in Image Lab 4.1 (Bio-RAD) to correct any rotation of the image and
541 exported as .tif for densitometry in FIJI (ImageJ 1.47n) (Schindelin et al., 2012, Schneider et al.,
542 2012). The lookup table (LUT) was inverted and images rotated 90 degrees. Using the rectangular
543 selection tool, a box was drawn around the lane of interest to encompass the full range of Bak signal
544 (with fixed dimensions of 370 x 50 pixels). This box was then measured with the Dynamic ROI
545 profiler plugin. Plot values were exported for analysis in Prism (ver 6.0f, Graphpad Software Co.,
546 La Jolla, CA, USA), and normalised to a fraction of the total intensity for each lane of interest. A
547 clearer representation of multiple replicate plots of lane intensity was achieved by a linear rescaling
548 of each replicate's horizontal axis so that the maximum corresponding to Bak 4x species, and the
549 characteristic minimum (which is a highly reproducible artefact of our Bak BNP western blots) at
550 ~720 kDa, coincided across replicates.

551 **Simulation of linkage between dimers (V61C:V61C')**

552 The formation of a disulphide linked oligomer is modelled by repeatedly (a) selecting an available
553 pair of cysteines on neighbouring dimers at random, (b) declaring them linked and (c) removing
554 those cysteines from the list of those subsequently available. We continue until no neighbouring
555 dimers have cysteines available for linkage, to reflect complete linkage of V61C:V61C'. We
556 consider a collection of Bak dimers on a two-dimensional surface (see Figure 6). Dimers are
557 arranged on a hexagonal grid, and linkage is permitted in all directions. Each dimer has two
558 cysteines available for disulphide linkage to a neighbouring dimer. We simulate such that linkage is
559 allowed in all directions with equal probability. Reduced linkage efficiency was modelled by

560 introducing an edge blocking effect. Every edge between neighbouring hexagonal cells was flagged
561 as eligible for a disulphide bond, independently at random with probability p constant across all
562 edges in a given simulation, for p=0, 0.25, 0.5 and 0.75. We modelled the experimental scenario
563 where Bak dimers were formed from a mixture of equal amounts of V61C and cys-null monomers
564 by assigning each dimer either zero, one or two available cysteines with probability 0.25, 0.5 and
565 0.25 respectively (see Figure S5C).

566 Predicted densitometry for each Bak dimer multiplicity are presented by taking the distribution of
567 oligomer sizes on completion of the simulation, multiplying by the number of Bak dimers in each
568 oligomer to obtain the theoretical density that would give rise to in the western blot, using an
569 exponential horizontal axis to mimic the nonlinear spacing of bands, and applying a gaussian kernel
570 estimator to approximate the smearing of bands and their running into one another at higher
571 molecular weights (see Figure S4).

572 **AUTHOR CONTRIBUTIONS**

573 Conceptualization, RTU, GD, RMK; Methodology, RTU, MOH, SI, GD, RMK; Software, MOH;
574 Investigation, RTU, SI, RB, JMB, AEA, GD; Formal analysis, RTU, MOH; Data curation, MOH;
575 Visualization, RTU, MOH, SI, RMK; Writing – Original Draft, RTU, RMK; Writing – Review &
576 Editing, RTU, MOH, SI, AEA, GD, RMK; Supervision, RTU, RMK

577 **ACKNOWLEDGMENTS**

578 The authors declare no conflict of interest. We thank Peter Colman, Peter Czabotar, John Markham,
579 Matthew Ritchie, Aline Oelgeklaus and Melissa Shi for critical comments on the manuscript. We
580 thank Colin Hockings for helpful discussions regarding simulations. We gratefully acknowledge the
581 IASD labelling assay development and analysis methods of Dana Westphal. Our work is supported
582 by NHMRC grants (637337 and 1016701), and the Victorian State Government Operational
583 Infrastructure Support and the Australian Government NHMRC IRIISS.

584 **REFERENCES**

585 ALSOP, A. E., FENNELL, S. C., BARTOLO, R. C., TAN, I. K., DEWSON, G. & KLUCK, R. M.
586 2015. Dissociation of Bak alpha1 helix from the core and latch domains is required for
587 apoptosis. *Nat Commun,* 6**,** 6841.
588 ALUVILA, S. M., T. HUSTEDT, E. FAJER, P. CHOE, JY. OH, KJ. 2014. Organization of the
589 mitochondrial apoptotic BAK pore: oligomerization of the Bak homodimers. *J Biol Chem,*
590 289**,** 2537-51.
591 BLEICKEN, S., JESCHKE, G., STEGMUELLER, C., SALVADOR-GALLEGO, R., GARCIA-
592 SAEZ, A. J. & BORDIGNON, E. 2014. Structural model of active bax at the membrane.
593 *Mol Cell,* 56**,** 496-505.
594 BROUWER, J. M., WESTPHAL, D., DEWSON, G., ROBIN, A. Y., UREN, R. T., BARTOLO, R.,
595 THOMPSON, G. V., COLMAN, P. M., KLUCK, R. M. & CZABOTAR, P. E. 2014. Bak
596 Core and Latch Domains Separate during Activation, and Freed Core Domains Form
597 Symmetric Homodimers. *Mol Cell,* 55**,** 938-46.
598 CHEN, F. Y., LEE, M. T. & HUANG, H. W. 2003. Evidence for membrane thinning effect as the
599 mechanism for peptide-induced pore formation. *Biophys J,* 84**,** 3751-8.
600 CHEN, L., WILLIS, S. N., WEI, A., SMITH, B. J., FLETCHER, J. I., HINDS, M. G., COLMAN,
601 P. M., DAY, C. L., ADAMS, J. M. & HUANG, D. C. 2005. Differential targeting of
602 prosurvival Bcl-2 proteins by their BH3-only ligands allows complementary apoptotic
603 function. *Molecular Cell,* 17**,** 393-403.
604 CHENG, E. H., SHEIKO, T. V., FISHER, J. K., CRAIGEN, W. J. & KORSMEYER, S. J. 2003.
605 VDAC2 inhibits BAK activation and mitochondrial apoptosis. *Science,* 301**,** 513-517.
606 CZABOTAR, P. E., WESTPHAL, D., DEWSON, G., MA, S., HOCKINGS, C., FAIRLIE, W. D.,
607 LEE, E. F., YAO, S., ROBIN, A. Y., SMITH, B. J., HUANG, D. C., KLUCK, R. M.,
608 ADAMS, J. M. & COLMAN, P. M. 2013. Bax Crystal Structures Reveal How BH3
609 Domains Activate Bax and Nucleate Its Oligomerization to Induce Apoptosis. *Cell,* 152**,**
610 519-31.
611 DAI, H., SMITH, A., MENG, X. W., SCHNEIDER, P. A., PANG, Y. P. & KAUFMANN, S. H.
612 2011. Transient binding of an activator BH3 domain to the Bak BH3-binding groove
613 initiates Bak oligomerization. *J Cell Biol,* 194**,** 39-48.
614 DEWSON, G., KRATINA, T., CZABOTAR, P., DAY, C. L., ADAMS, J. M. & KLUCK, R. M.
615 2009. Bak activation for apoptosis involves oligomerization of dimers via their alpha6
616 helices. *Mol Cell,* 36**,** 696-703.
617 DEWSON, G., KRATINA, T., SIM, H. W., PUTHALAKATH, H., ADAMS, J. M., COLMAN, P.
618 M. & KLUCK, R. M. 2008. To trigger apoptosis Bak exposes its BH3 domain and homo-
619 dimerizes via BH3:grooove interactions. *Mol Cell,* 30**,** 369-380.
620 DEWSON, G., MA, S., FREDERICK, P., HOCKINGS, C., TAN, I., KRATINA, T. & KLUCK, R.
621 M. 2012. Bax dimerizes via a symmetric BH3:groove interface during apoptosis. *Cell Death*
622 *Differ,* 19**,** 661-70.
623 DU, H., WOLF, J., SCHAFER, B., MOLDOVEANU, T., CHIPUK, J. E. & KUWANA, T. 2011.
624 BH3 domains other than Bim and Bid can directly activate Bax/Bak. *J Biol Chem,* 286**,** 491-
625 501.
626 FERRER, P. E., FREDERICK, P., GULBIS, J. M., DEWSON, G. & KLUCK, R. M. 2012.
627 Translocation of a Bak C-terminus mutant from cytosol to mitochondria to mediate
628 cytochrome C release: implications for Bak and Bax apoptotic function. *PLoS One,* 7**,**
629 e31510.
630 GAHL, R. F., HE, Y., YU, S. & TJANDRA, N. 2014. Conformational rearrangements in the pro-
631 apoptotic protein, Bax, as it inserts into mitochondria: a cellular death switch. *J Biol Chem,*
632 289**,** 32871-82.
633 GARCIA-SAEZ, A. J. 2012. The secrets of the Bcl-2 family. *Cell Death Differ,* 19**,** 1733-40.

634 GAVATHIOTIS, E., REYNA, D. E., DAVIS, M. L., BIRD, G. H. & WALENSKY, L. D. 2010.
635 BH3-Triggered Structural Reorganization Drives the Activation of Proapoptotic BAX.
636 *Molecular Cell,* 40**,** 481-92.
637 GEORGE, N. M., EVANS, J. J. & LUO, X. 2007. A three-helix homo-oligomerization domain
638 containing BH3 and BH1 is responsible for the apoptotic activity of Bax. *Genes Dev,* 21**,**
639 1937-1948.
640 GILBERT, R. J. 2016. Protein-lipid interactions and non-lamellar lipidic structures in membrane
641 pore formation and membrane fusion. *Biochim Biophys Acta,* 1858**,** 487-99.
642 GRIFFITHS, G. J., DUBREZ, L., MORGAN, C. P., JONES, N. A., WHITEHOUSE, J., CORFE,
643 B. M., DIVE, C. & HICKMAN, J. A. 1999. Cell damage-induced conformational changes
644 of the pro-apoptotic protein Bak in vivo precede the onset of apoptosis. *Journal of Cell*
645 *Biology,* 144**,** 903-914.
646 GROSSE, L., WURM, C. A., BRUSER, C., NEUMANN, D., JANS, D. C. & JAKOBS, S. 2016.
647 Bax assembles into large ring-like structures remodeling the mitochondrial outer membrane
648 in apoptosis. *EMBO J,* 35**,** 402-13.
649 GRUNDLING, A., BLASI, U. & YOUNG, R. 2000. Biochemical and genetic evidence for three
650 transmembrane domains in the class I holin, lambda S. *J Biol Chem,* 275**,** 769-76.
651 HOCKINGS, C., ANWARI, K., NINNIS, R. L., BROUWER, J., O'HELY, M., EVANGELISTA,
652 M., HINDS, M. G., CZABOTAR, P. E., LEE, E. F., FAIRLIE, W. D., DEWSON, G. &
653 KLUCK, R. M. 2015. Bid chimeras indicate that most BH3-only proteins can directly
654 activate Bak and Bax, and show no preference for Bak versus Bax. *Cell Death Dis,* 6**,**
655 e1735.
656 IYER, S., BELL, F., WESTPHAL, D., ANWARI, K., GULBIS, J., SMITH, B. J., DEWSON, G. &
657 KLUCK, R. M. 2015. Bak apoptotic pores involve a flexible C-terminal region and
658 juxtaposition of the C-terminal transmembrane domains. *Cell Death Differ*.
659 KLUCK, R. M., ESPOSTI, M. D., PERKINS, G., RENKEN, C., KUWANA, T., BOSSY-
660 WETZEL, E., GOLDBERG, M., ALLEN, T., BARBER, M. J., GREEN, D. R. &
661 NEWMEYER, D. D. 1999. The pro-apoptotic proteins, Bid and Bax, cause a limited
662 permeabilization of the mitochondrial outer membrane that is enhanced by cytosol. *J Cell*
663 *Biol,* 147**,** 809-22.
664 LAZAROU, M., STOJANOVSKI, D., FRAZIER, A. E., KOTEVSKI, A., DEWSON, G.,
665 CRAIGEN, W. J., KLUCK, R. M., VAUX, D. L. & RYAN, M. T. 2010. Inhibition of Bak
666 activation by VDAC2 is dependent on the Bak transmembrane anchor. *J Biol Chem,* 285**,**
667 36876-83.
668 LEE, E. F., GRABOW, S., CHAPPAZ, S., DEWSON, G., HOCKINGS, C., KLUCK, R. M.,
669 GRAY, D. H., WITKOWSKI, M. T., EVANGELISTA, M., PETTIKIRIARACHCHI, A.,
670 BOUILLET, P., CORY, S., VANDENBERG, C. J., LANE, R. M., CZABOTAR, P. E.,
671 COLMAN, P. M., SMITH, B. J., KILE, B. T. & FAIRLIE, W. D. 2016. Physiological
672 restraint of Bak by Bcl-xL is essential for cell survival. *Genes Dev,* In press.
673 LEE, M. T., HUNG, W. C., CHEN, F. Y. & HUANG, H. W. 2008. Mechanism and kinetics of pore
674 formation in membranes by water-soluble amphipathic peptides. *Proc Natl Acad Sci U S A,*
675 105**,** 5087-92.
676 LEE, M. T., SUN, T. L., HUNG, W. C. & HUANG, H. W. 2013. Process of inducing pores in
677 membranes by melittin. *Proc Natl Acad Sci U S A,* 110**,** 14243-8.
678 LESHCHINER, E. S., BRAUN, C. R., BIRD, G. H. & WALENSKY, L. D. 2013. Direct activation
679 of full-length proapoptotic BAK. *Proc Natl Acad Sci U S A,* 110**,** E986-95.
680 LINDSTEN, T., ROSS, A. J., KING, A., ZONG, W., RATHMELL, J. C., SHIELS, H. A.,
681 ULRICH, E., WAYMIRE, K. G., MAHAR, P., FRAUWIRTH, K., CHEN, Y., WEI, M.,
682 ENG, V. M., ADELMAN, D. M., SIMON, M. C., MA, A., GOLDEN, J. A., EVAN, G.,
683 KORSMEYER, S. J., MACGREGOR, G. R. & THOMPSON, C. B. 2000. The combined
684 functions of proapoptotic Bcl-2 family members Bak and Bax are essential for normal
685 development of multiple tissues. *Mol Cell,* 6**,** 1389-1399.

686 LLAMBI, F., MOLDOVEANU, T., TAIT, S. W., BOUCHIER-HAYES, L., TEMIROV, J.,
687 MCCORMICK, L. L., DILLON, C. P. & GREEN, D. R. 2011. A unified model of
688 mammalian BCL-2 protein family interactions at the mitochondria. *Mol Cell,* 44**,** 517-31.
689 LUO, L., YANG, J. & LIU, D. 2014. Integration and oligomerization of Bax protein in lipid
690 bilayers characterized by single molecule fluorescence study. *J Biol Chem,* 289**,** 31708-18.
691 MA, S., HOCKINGS, C., ANWARI, K., KRATINA, T., FENNELL, S., LAZAROU, M., RYAN,
692 M. T., KLUCK, R. M. & DEWSON, G. 2013. Assembly of the Bak apoptotic pore: a
693 critical role for the Bak protein alpha6 helix in the multimerization of homodimers during
694 apoptosis. *J Biol Chem,* 288**,** 26027-38.
695 MA, S. B., NGUYEN, T. N., TAN, I., NINNIS, R., IYER, S., STROUD, D. A., MENARD, M.,
696 KLUCK, R. M., RYAN, M. T. & DEWSON, G. 2014. Bax targets mitochondria by distinct
697 mechanisms before or during apoptotic cell death: a requirement for VDAC2 or Bak for
698 efficient Bax apoptotic function. *Cell Death Differ*.
699 MOLDOVEANU, T., LIU, Q., TOCILJ, A., WATSON, M. H., SHORE, G. & GEHRING, K. 2006.
700 The x-ray structure of a BAK homodimer reveals an inhibitory zinc binding site. *Molecular*
701 *Cell,* 24**,** 677-688.
702 MUELLER, M., GRAUSCHOPF, U., MAIER, T., GLOCKSHUBER, R. & BAN, N. 2009. The
703 structure of a cytolytic alpha-helical toxin pore reveals its assembly mechanism. *Nature,*
704 459**,** 726-30.
705 NASU, Y., BENKE, A., ARAKAWA, S., YOSHIDA, G. J., KAWAMURA, G., MANLEY, S.,
706 SHIMIZU, S. & OZAWA, T. 2016. In Situ Characterization of Bak Clusters Responsible
707 for Cell Death Using Single Molecule Localization Microscopy. *Sci Rep,* 6**,** 27505.
708 NECHUSHTAN, A., SMITH, C. L., LAMENSDORF, I., YOON, S. H. & YOULE, R. J. 2001. Bax
709 and Bak coalesce into novel mitochondria-associated clusters during apoptosis. *Journal of*
710 *Cell Biology,* 153**,** 1265-1276.
711 PANG, Y. P., DAI, H., SMITH, A., MENG, X. W., SCHNEIDER, P. A. & KAUFMANN, S. H.
712 2012. Bak Conformational Changes Induced by Ligand Binding: Insight into BH3 Domain
713 Binding and Bak Homo-Oligomerization. *Sci Rep,* 2**,** 257.
714 SALVADOR-GALLEGO, R., MUND, M., COSENTINO, K., SCHNEIDER, J., UNSAY, J.,
715 SCHRAERMEYER, U., ENGELHARDT, J., RIES, J. & GARCIA-SAEZ, A. J. 2016. Bax
716 assembly into rings and arcs in apoptotic mitochondria is linked to membrane pores. *EMBO*
717 *J,* 35**,** 389-401.
718 SATSOURA, D., KUCERKA, N., SHIVAKUMAR, S., PENCER, J., GRIFFITHS, C., LEBER, B.,
719 ANDREWS, D. W., KATSARAS, J. & FRADIN, C. 2012. Interaction of the full-length
720 Bax protein with biomimetic mitochondrial liposomes: a small-angle neutron scattering and
721 fluorescence study. *Biochim Biophys Acta,* 1818**,** 384-401.
722 SCHINDELIN, J., ARGANDA-CARRERAS, I., FRISE, E., KAYNIG, V., LONGAIR, M.,
723 PIETZSCH, T., PREIBISCH, S., RUEDEN, C., SAALFELD, S., SCHMID, B., TINEVEZ,
724 J. Y., WHITE, D. J., HARTENSTEIN, V., ELICEIRI, K., TOMANCAK, P. & CARDONA,
725 A. 2012. Fiji: an open-source platform for biological-image analysis. *Nat Methods,* 9**,** 676-
726 82.
727 SCHNEIDER, C. A., RASBAND, W. S. & ELICEIRI, K. W. 2012. NIH Image to ImageJ: 25 years
728 of image analysis. *Nat Methods,* 9**,** 671-5.
729 SONG, L., HOBAUGH, M. R., SHUSTAK, C., CHELEY, S., BAYLEY, H. & GOUAUX, J. E.
730 1996. Structure of staphylococcal alpha-hemolysin, a heptameric transmembrane pore.
731 *Science,* 274**,** 1859-66.
732 SUBBURAJ, Y., COSENTINO, K., AXMANN, M., PEDRUEZA-VILLALMANZO, E.,
733 HERMANN, E., BLEICKEN, S., SPATZ, J. & GARCIA-SAEZ, A. J. 2015. Bax monomers
734 form dimer units in the membrane that further self-assemble into multiple oligomeric
735 species. *Nat Commun,* 6**,** 8042.

736 SUNG, T. C., LI, C. Y., LAI, Y. C., HUNG, C. L., SHIH, O., YEH, Y. Q., JENG, U. S. &
737 CHIANG, Y. W. 2015. Solution Structure of Apoptotic BAX Oligomer: Oligomerization
738 Likely Precedes Membrane Insertion. *Structure,* 23**,** 1878-88.
739 SUZUKI, M., YOULE, R. J. & TJANDRA, N. 2000. Structure of Bax: coregulation of dimer
740 formation and intracellular localization. *Cell,* 103**,** 645-654.
741 TERRONES, O., ANTONSSON, B., YAMAGUCHI, H., WANG, H. G., LIU, J., LEE, R. M.,
742 HERRMANN, A. & BASANEZ, G. 2004. Lipidic pore formation by the concerted action of
743 proapoptotic BAX and tBID. *J Biol Chem,* 279**,** 30081-30091.
744 TRAN, V. H., BARTOLO, R., WESTPHAL, D., ALSOP, A., DEWSON, G. & KLUCK, R. M.
745 2013. Bak apoptotic function is not directly regulated by phosphorylation. *Cell Death Dis,* 4**,**
746 e452.
747 WEBER, K., HARPER, N., SCHWABE, J. & COHEN, G. M. 2013. BIM-mediated membrane
748 insertion of the BAK pore domain is an essential requirement for apoptosis. *Cell Rep,* 5**,**
749 409-20.
750 WEI, M. C., ZONG, W. X., CHENG, E. H., LINDSTEN, T., PANOUTSAKOPOULOU, V.,
751 ROSS, A. J., ROTH, K. A., MACGREGOR, G. R., THOMPSON, C. B. & KORSMEYER,
752 S. J. 2001. Proapoptotic BAX and BAK: a requisite gateway to mitochondrial dysfunction
753 and death. *Science,* 292**,** 727-730.
754 WESTPHAL, D., DEWSON, G., MENARD, M., FREDERICK, P., IYER, S., BARTOLO, R.,
755 GIBSON, L., CZABOTAR, P. E., SMITH, B. J., ADAMS, J. M. & KLUCK, R. M. 2014.
756 Apoptotic pore formation is associated with in-plane insertion of Bak or Bax central helices
757 into the mitochondrial outer membrane. *Proc Natl Acad Sci U S A,* 111**,** E4076-85.
758 WOLTER, K. G., HSU, Y. T., SMITH, C. L., NECHUSHTAN, A., XI, X. G. & YOULE, R. J.
759 1997. Movement of Bax from the cytosol to mitochondria during apoptosis. *Journal of Cell*
760 *Biology,* 139**,** 1281-1292.
761 ZHANG, Z., SUBRAMANIAM, S., KALE, J., LIAO, C., HUANG, B., BRAHMBHATT, H.,
762 CONDON, S. G., LAPOLLA, S. M., HAYS, F. A., DING, J., HE, F., ZHANG, X. C., LI, J.,
763 SENES, A., ANDREWS, D. W. & LIN, J. 2016. BH3-in-groove dimerization initiates and
764 helix 9 dimerization expands Bax pore assembly in membranes. *EMBO J,* 35**,** 208-36.
765 ZHANG, Z., ZHU, W., LAPOLLA, S. M., MIAO, Y., SHAO, Y., FALCONE, M., BOREHAM,
766 D., MCFARLANE, N., DING, J., JOHNSON, A. E., ZHANG, X. C., ANDREWS, D. W. &
767 LIN, J. 2010. Bax forms an oligomer via separate, yet interdependent, surfaces. *J Biol*
768 *Chem,* 285**,** 17614-17627.
769 ZHOU, L. & CHANG, D. C. 2008. Dynamics and structure of the Bax-Bak complex responsible for
770 releasing mitochondrial proteins during apoptosis. *J Cell Sci,* 121**,** 2186-96.

771

772

Figure 1

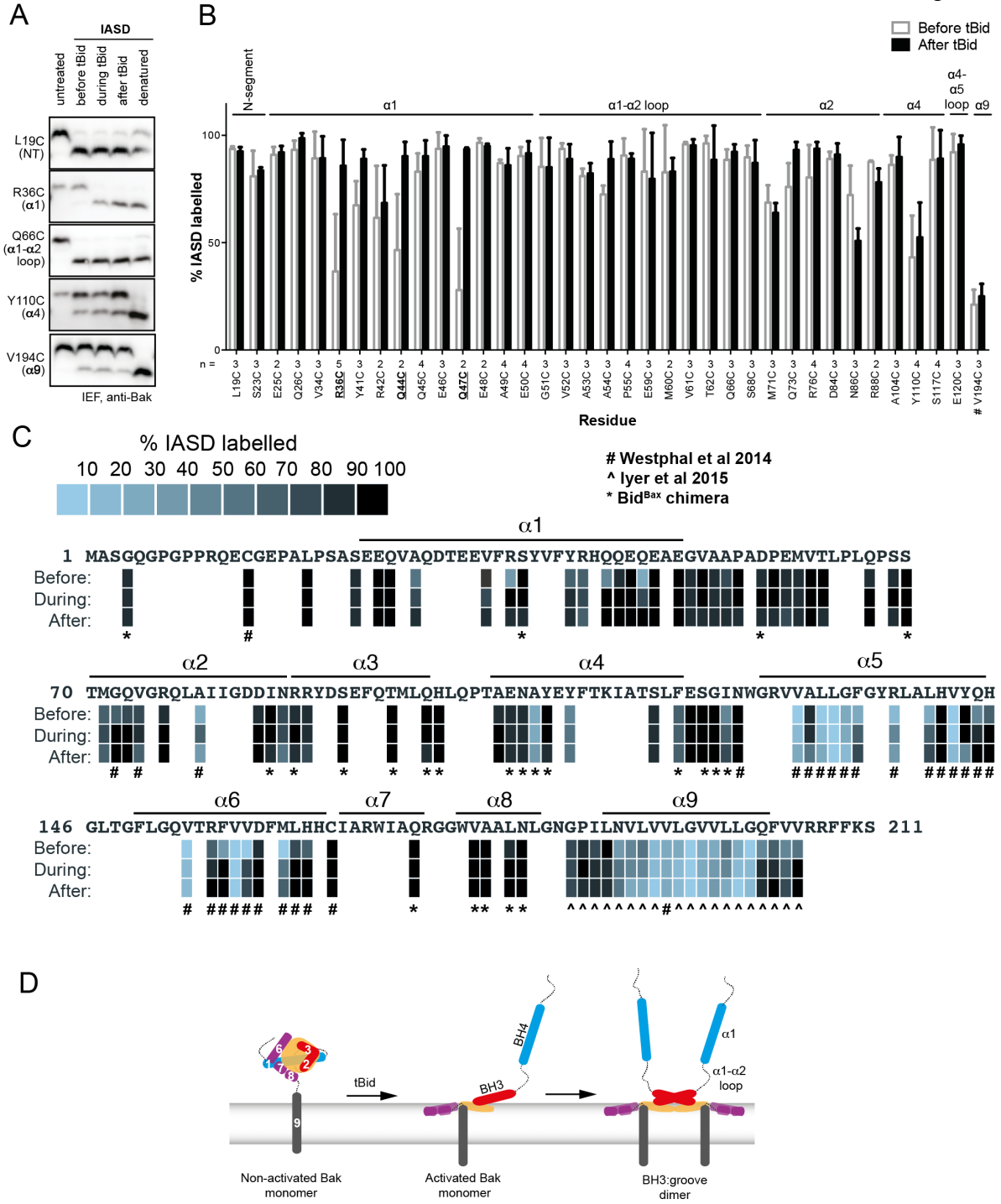

773

774

775 **Figure 1** Following oligomerization, the Bak N-segment, α1 and α1-α2 loop become fully solvent-
776 exposed in contrast to the partially exposed core (α2-α5) and latch (α6-α9).

777 (A) Solvent exposure of hBak cysteine mutants was assessed by IASD labelling before (lane 2),
778 during (lane 3) and after (lane 4) treatment with tBid. Controls of unlabelled (untreated, lane 1) and
779 fully labelled (denatured, lane 5) Bak were included for comparison. Example IEF western blots are
780 shown.

781 (B) Quantitation of IASD labelling before and after treatment with tBid for the panel of previously
782 untested Bak residues. Data are mean ± SD (n≥3), or range (n=2), with n for each residue labelled
783 on the x-axis. IASD labelling data for residue V194C were from (Westphal et al., 2014) (denoted
784 #). Residues for which there is a significant difference in IASD labelling before versus after tBid
785 are in bold and underlined ($p<0.05$).

786 (C) Heat map overview of Bak IASD labelling with tBid treatment from (B) pooled with published
787 analyses from (Westphal et al., 2014)(denoted #) or (Iyer et al., 2015)(denoted ^) and from
788 treatment with the $tBid^{Bax}$ chimera (denoted *; see also Figure S2).

789 (D) Schematic of Bak structural rearrangement from its non-activated monomeric state to the
790 activated dimer. Helices are numbered for the non-activated Bak. Note the complete solvent-
791 exposure of α1 and the α1-α2 loop in the activated dimer.

792

Figure 2

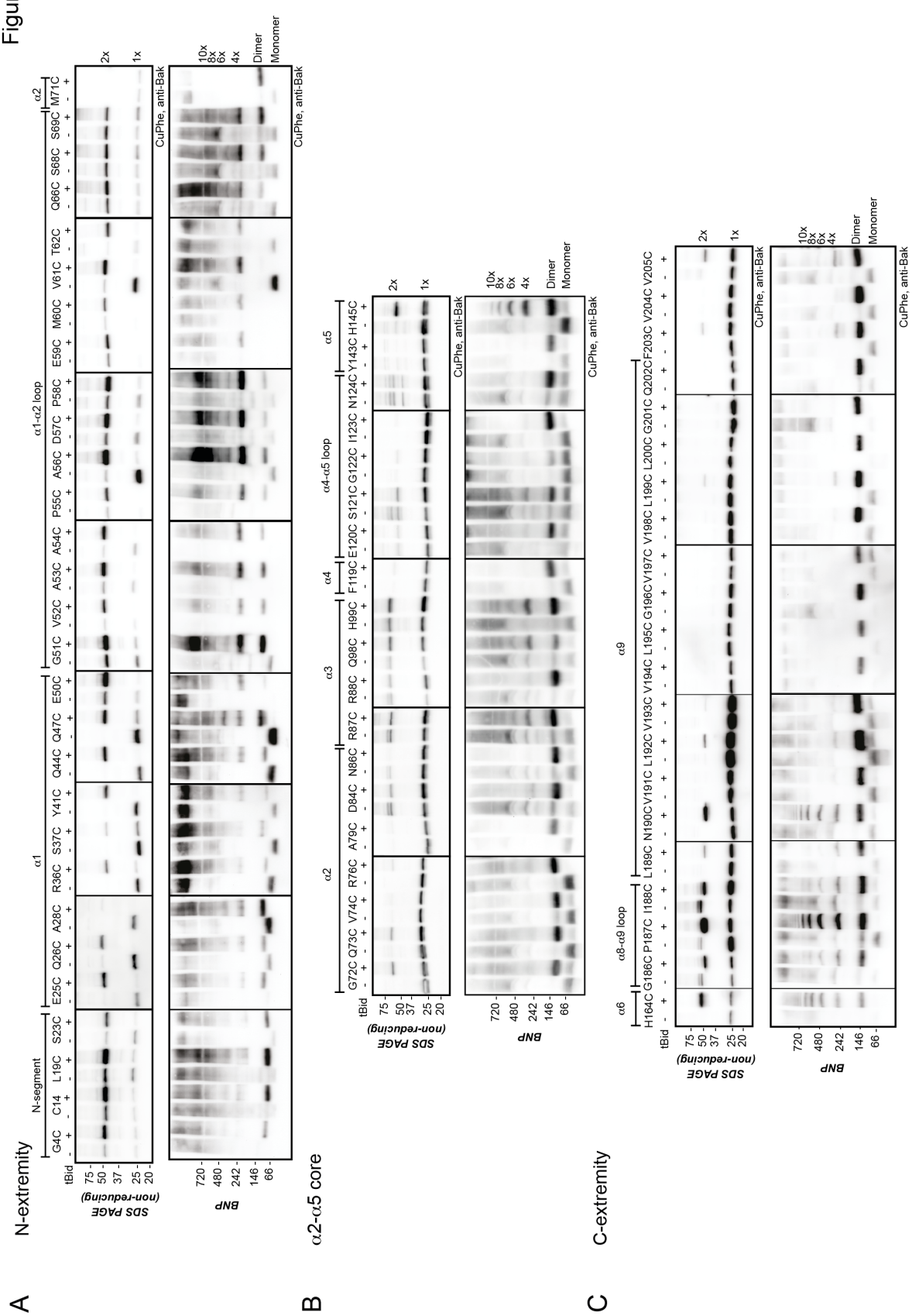

793
794
795
796

797 **Figure 2** The N- and C-extremities of oligomerized Bak are mobile relative to the α2-α5 core
798 dimer. Mitochondrial fractions from cells expressing the indicated Bak cysteine mutants were
799 incubated with tBid to oligomerize Bak, and oxidant (CuPhe) added to induce disulphide bonds.
800 Aliquots were analyzed by non-reducing SDS PAGE (upper panels) and BNP (lower panels), and
801 immunoblotted for Bak to detect linked species.

802 (A) Cysteine linkage occurs throughout the N-extremity.

803 (B) Cysteine linkage occurs, but is less complete, in the α2-α5 dimer core.

804 (C) Cysteine linkage occurs in the C-extremity. (See also α6:α6 linkage in (Dewson et al., 2008)
805 and α9:α9 linkage in (Iyer et al., 2015)).

806

807

Figure 3

A

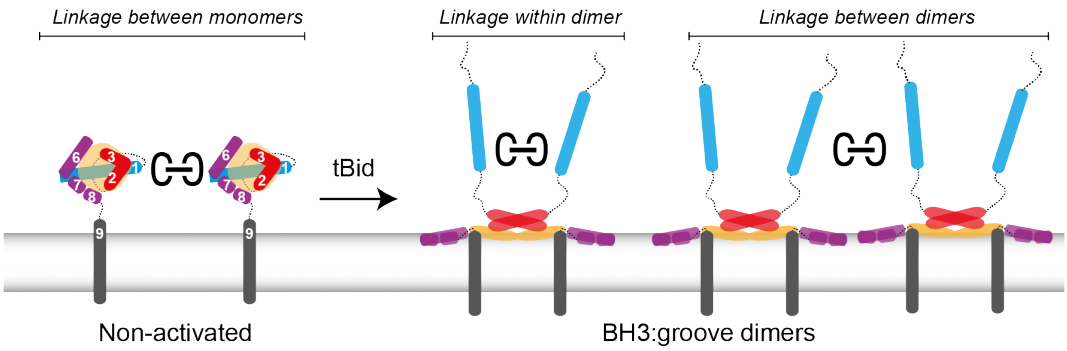

B

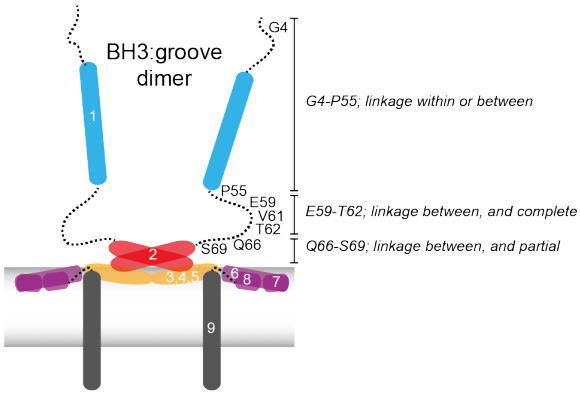

C

D

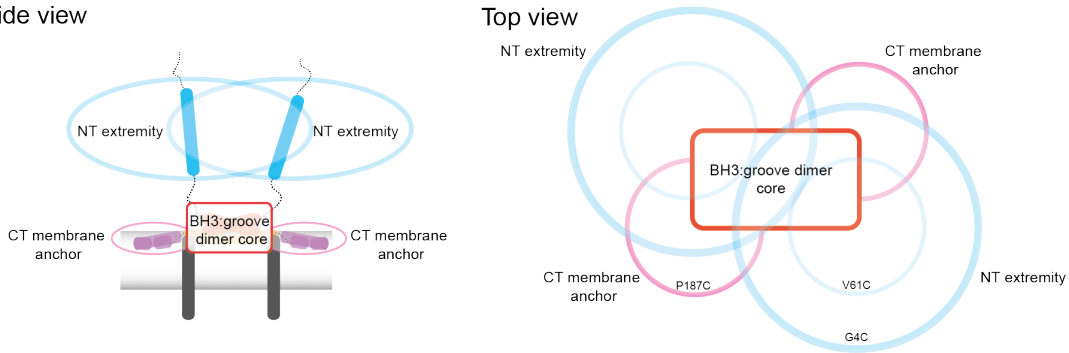

E

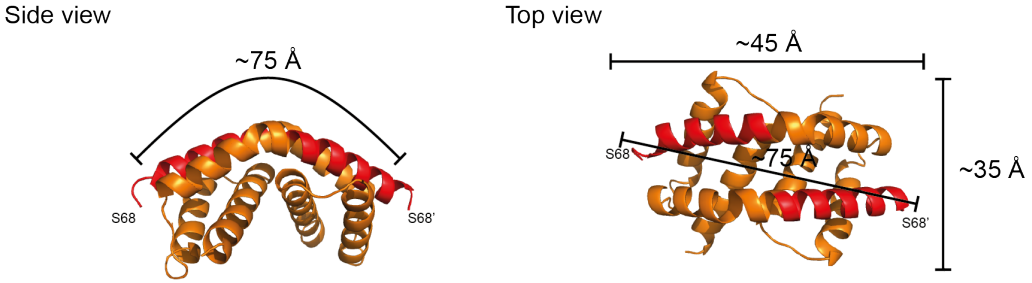

808

809 **Figure 3** Linkage constraints for different regions of the active Bak dimer support a flexible
810 extremity model for full-length Bak dimers in the MOM.

811 (A) The oxidant CuPhe induces linkage *between* Bak monomers or dimers, or *within* Bak dimers.
812 Correlation of BNP with non-reducing SDS PAGE can differentiate linkage within and between
813 dimers.

814 (B) Summary of linkage outcomes within or between dimers for residues in the Bak dimer N-
815 extremity.

816 (C) Linkage at the lateral corners of the Bak α2-α5 core dimer is highlighted with residue labels and
817 sticks on the crystal structure (4U2V (Brouwer et al., 2014)).

818 (D) Schematic of the activated Bak dimer at the membrane in side and top views. The range of
819 movement of the N- and C-extremities is indicated with coloured ovals (blue and pink respectively).

820 (E) Our linkage data are consistent with the dimensions of the Bak core dimer. The dimensions of
821 the Bak α2-α5 core dimer 4U2V (Brouwer et al., 2014) are shown in side view and top view. In the
822 crystal structure, the distance from one edge of the core at S68 over the bended structure of the
823 symmetric core to the opposing S68' is ~75 Å. Thus, for residues in the mobile N-extremity to link
824 within the core dimer, the two homotypic cysteine residues must bridge a distance of ~75 Å. This is
825 not feasible for the residue V61C which is ~30 Å from the symmetric core.

826

827

Figure 4

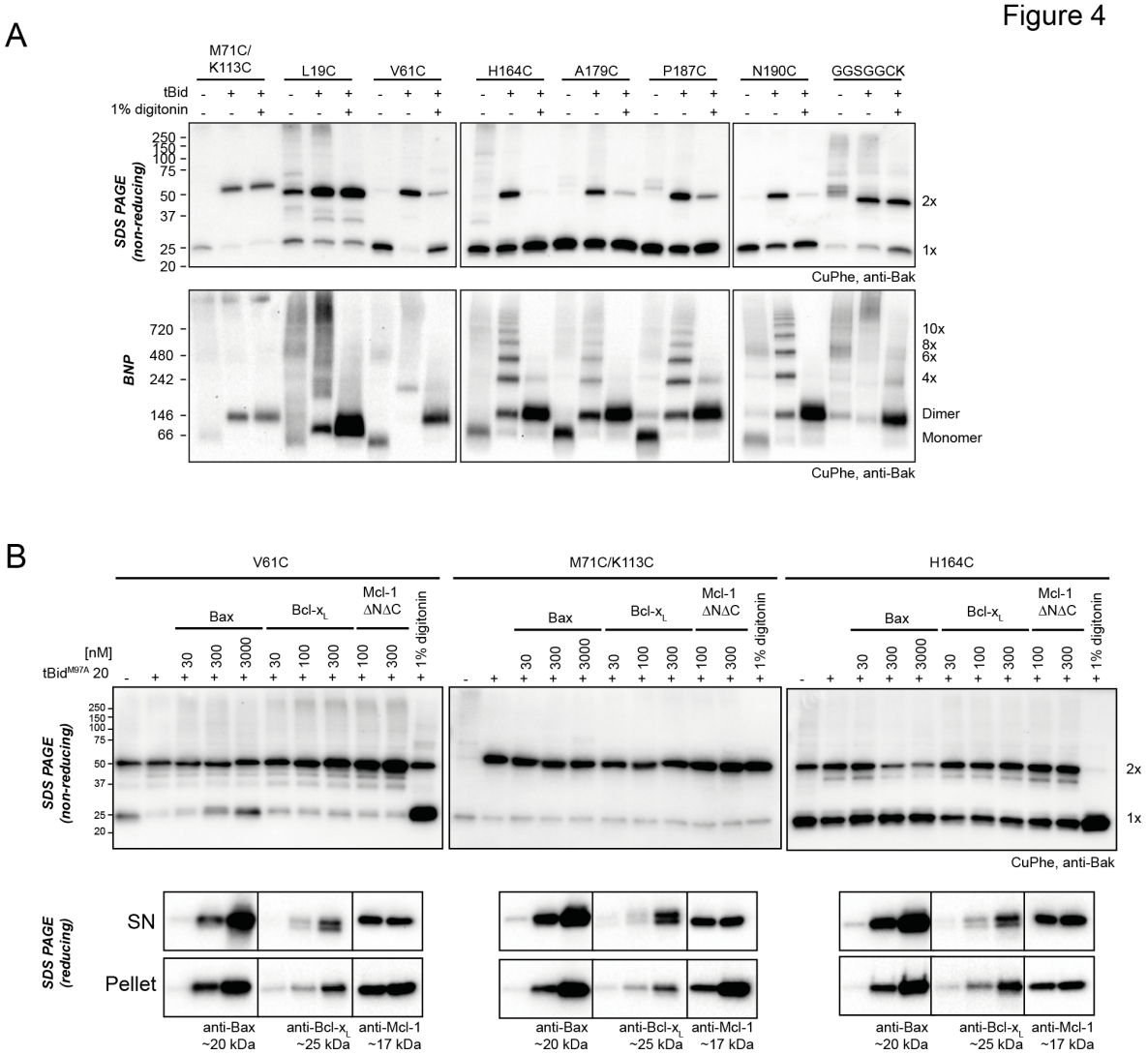

Figure 4 Bak dimer-dimer interactions are disrupted by detergent or Bax.

(A) Digitonin prevents linkage between Bak dimers. Membrane fractions expressing the indicated Bak single-cysteine variants were first treated with tBid, and then supplemented, as indicated, with detergent (1% digitonin) prior to cysteine linkage. Two additional mutants were included to show linkage within dimers at the BH3:groove interface (M71C/K113C) and at extensions to the C-terminus (GGSGGCK).

(B) Bax can disrupt Bak dimer-dimer association. Membrane fractions first treated with $tBid^{M97A}$ were then incubated, as indicated, with Bax, Bcl-x_L, Mcl-1ΔN151ΔC23 or digitonin prior to cysteine linkage (upper panels). Supernatant and pellet fractions showed partial translocation of each recombinant protein to the membrane fraction (lower panels).

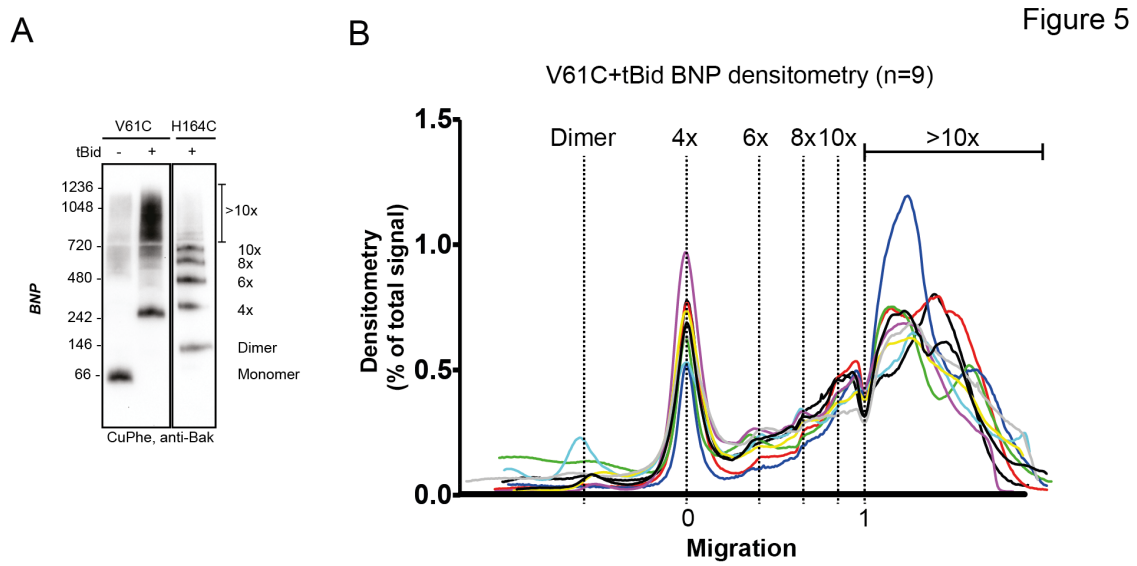

Figure 5 V61C:V61C' linkage is a marker of dimer-dimer interaction.

(A) BNP analysis of V61C:V61C' linkage revealed no dimers, and a high proportion of 4x and >10x species. In contrast, H164C:H164C' linkage revealed a ladder of linked species.

(B) Densitometry of V61C:V61C' BNP linkage in Bak oligomers shows negligible dimers but reproducible linked species at 4x, 6x, 8x, and 10x, and a large population of species >10x. Densitometry data (n=9) were normalised to the area under the curve after alignment as described in Experimental Procedures. To correct for small variations in electrophoretic migration, we employed a noise reduction algorithm in which the 4x peak (0) and a minima at ~720 kDa (1) were aligned between replicates.

Figure 6

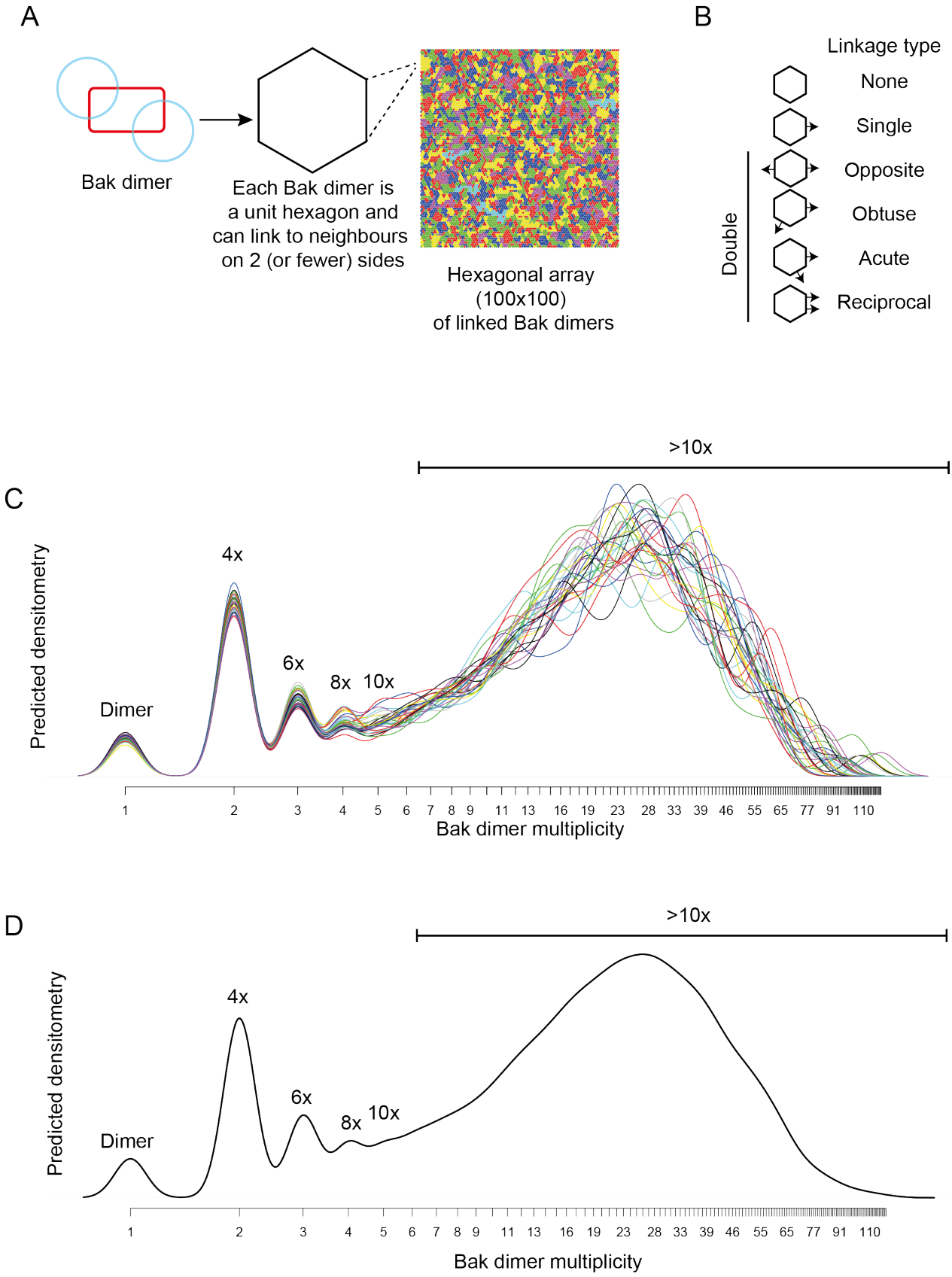

853

854

855

Figure 6 Bak dimer arrangement examined by two-dimensional stochastic simulations: a random arrangement is the best fit for the V61C:V61C' BNP linkage densitometry.

(A) A grid of 100x100 was designated for the 2D simulations. Each unit hexagon within that grid represented a Bak dimer, with the capacity to link to 2 neighbouring hexagons. The direction of linkage from each hexagon was randomised. An example visual output from a 100x100 hexagonal array is shown: neighbouring subsets of linked Bak dimers within the grid are delineated by different colours.

(B) Linkage possibilities between each dimer unit in a hexagonal 2D array.

(C,D) Overlay (C), and average (D) of 30 predicted densitometry plots.

867

Figure 7

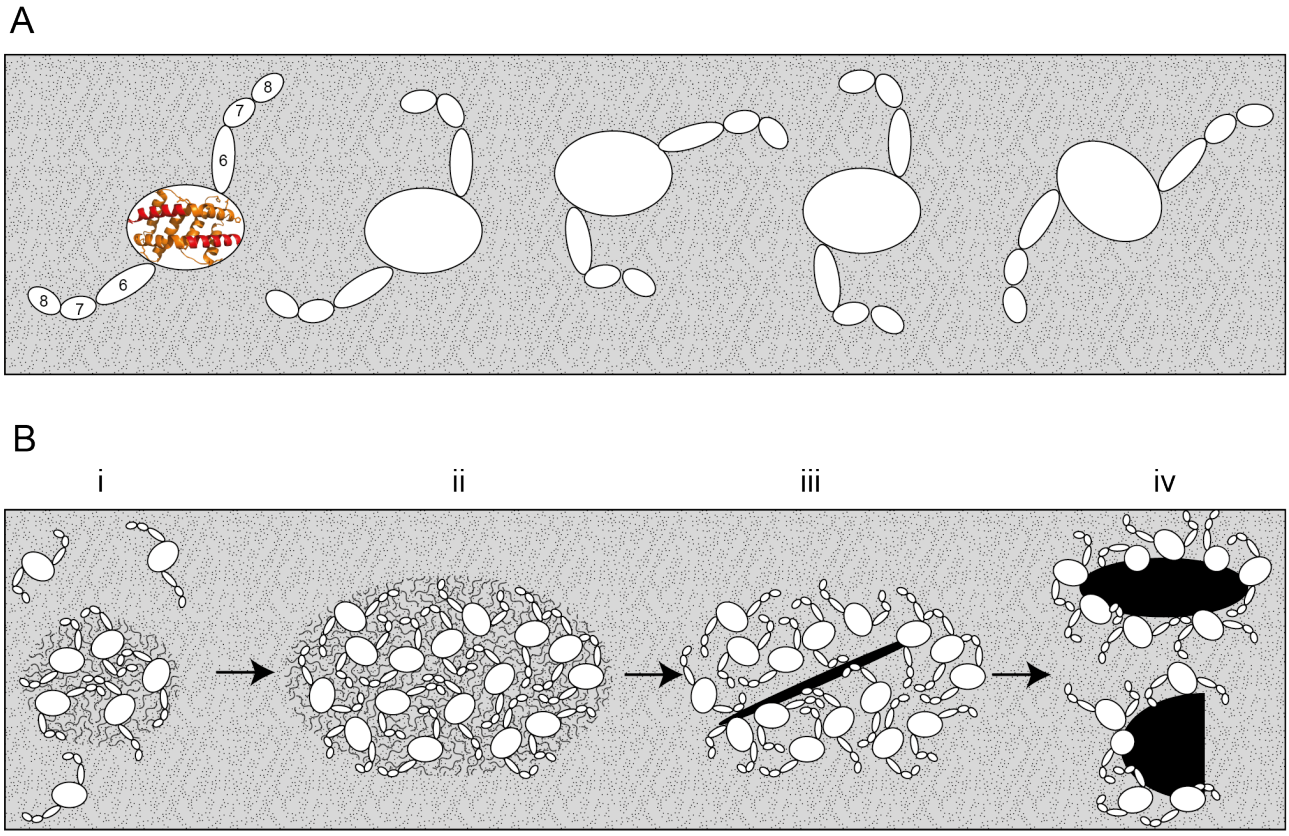

868

869 **Figure 7** Bak dimers adopt various conformations on the membrane surface and aggregate in
870 compact, disordered clusters to disrupt the mitochondrial outer membrane.

871 (A) The top view of Bak dimers lying in-plane on the mitochondrial surface. The α2-α5 core is
872 bounded by the large oval. Extending from the core are the membrane anchored C-terminal helices
873 α6, α7 and α8. For simplicity, the α9 transmembrane domains that project into the membrane plane,
874 and the flexible, solvent exposed N-termini of each dimer are not shown.

875 (B) Growing clusters of Bak dimers induce membrane tension to rupture mitochondria.

876 (i) Upon activation, Bak dimers penetrate the outer leaflet of the membrane and accumulate in a
877 compact, irregular cluster.

878 (ii) More dimers converge on the cluster, thus enlarging the patch of membrane disturbance.

879 (iii) Once the patch attains a critical area, a non-lamellar lipidic arrangement is generated, relieving
880 membrane tension.

881 (iv) Lipids and Bak dimers rearrange to bury exposed hydrophobic surfaces, yielding a variety of
882 proteolipid (toroidal) "pores". Our assays survey a mixture of Bak linkage products derived from
883 stages (ii), (iii) and (iv).

884 **SUPPLEMENTAL INFORMATION**

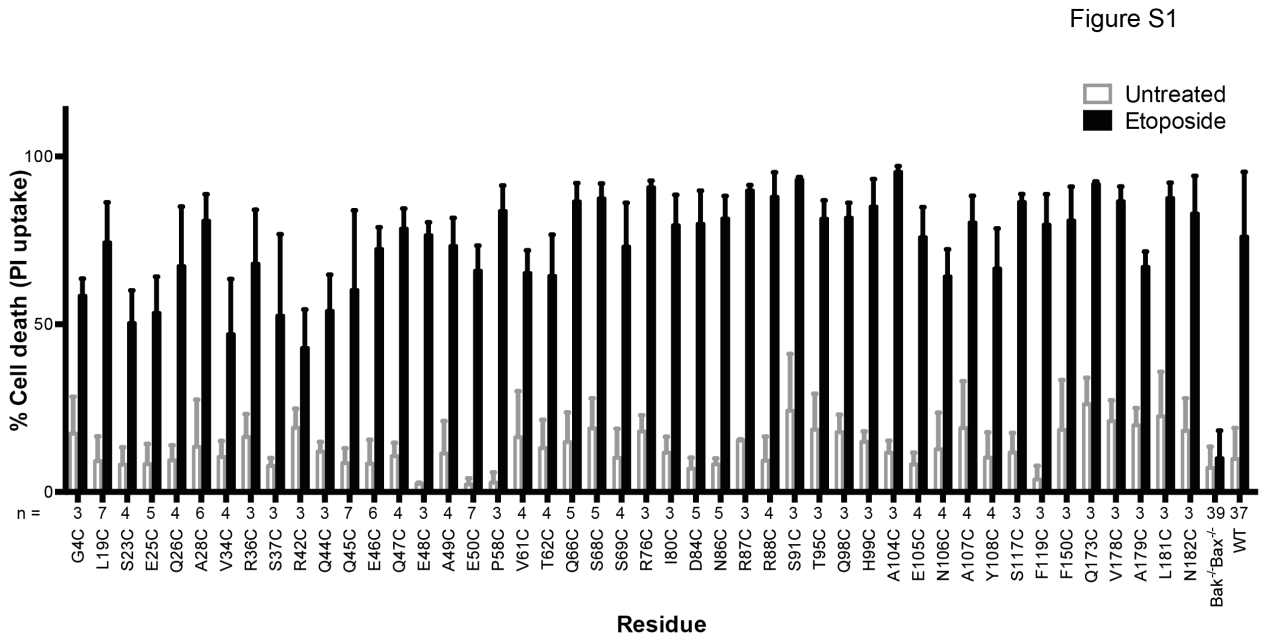

885

886 **Figure S1** Bak cysteine variants retain apoptotic function. *Bak*$^{-/-}$*Bax*$^{-/-}$ MEF expressing Bak cysteine
887 variants were treated with 10 μM etoposide for 24 h and the percentage cell death quantified by
888 propidium iodide uptake. Data are for unpublished mutants only and are the mean ± SD. The
889 number of replicates (n) for each residue is labelled on the x-axis.

Figure S2

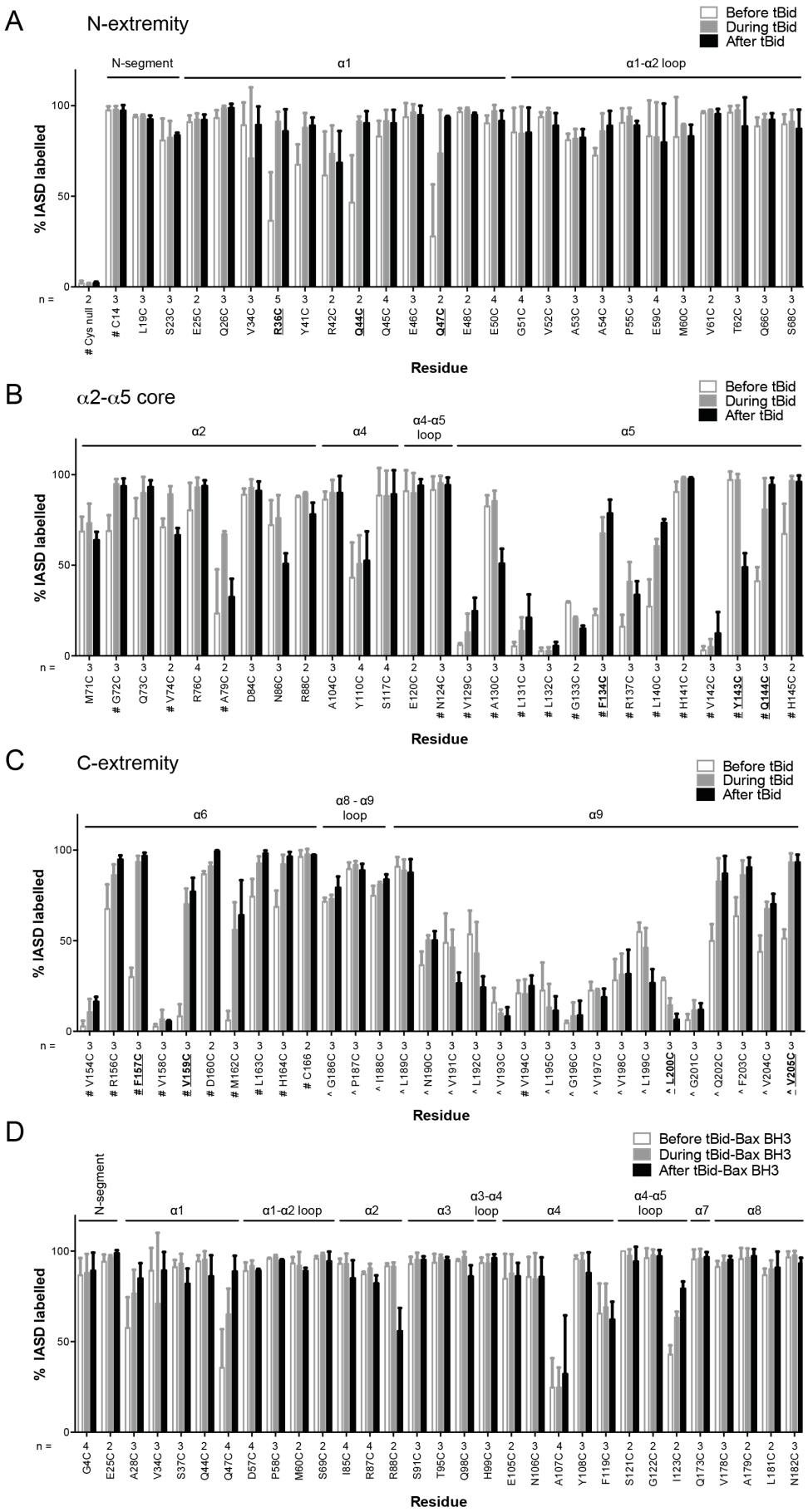
A
N-extremity
Before tBid
During tBid
After tBid
N-segment
α1
α1-α2 loop
% IASD labelled
Residue
B
α2-α5 core
α2
α4
α4-α5 loop
α5
C
C-extremity
α6
α8 - α9 loop
α9
D
Before tBid-Bax BH3
During tBid-Bax BH3
After tBid-Bax BH3
α2
α3
α3-α4 loop
α4
α4-α5 loop
α7
α8

892 **Figure S2** Quantitation of Bak IASD labelling before, during and after Bak activation.

893 (A,B,C). Labelling before, during or after treatment with tBid, segregated by Bak N-extremity (A),
894 Core (B), and C-extremity (C). Previously untested Bak residues have been pooled with data from
895 previous studies (# denotes data from (Westphal et al., 2014), ^ denotes data from (Iyer et al.,
896 2015)). Data are mean ± SD, or range (n=2), with n for each residue labelled on the x-axis.
897 Residues for which there is a significant difference in IASD labelling before versus after tBid are in
898 bold and underlined ($p<0.05$).

899 (D) IASD labelling for selected Bak variants before, during and after treatment with $tBid^{Bax}$
900 chimera (Hockings et al., 2015). Data are mean ± SD ($n \geq 3$), or range (n=2), with n for each
901 residue labelled on the x-axis. No significant differences (p value cutoff of 0.05) in IASD labelling
902 before versus after $tBid^{Bax}$ were observed.

903

904

905

Figure S3

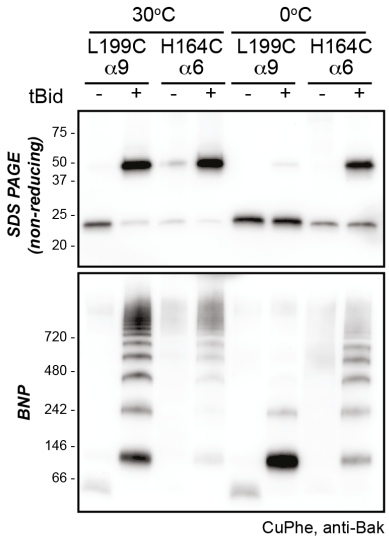

906

907 **Figure S3** Higher temperature enhances disulphide bonding of cysteine residues in α6 (H164C) and
908 the α9 transmembrane domain (L199C). Mitochondrial fractions from cells expressing the indicated
909 Bak cysteine mutants were incubated with tBid to oligomerize Bak, and oxidant (CuPhe) added to
910 induce disulphide bonds. Samples were incubated with CuPhe for 15 min either at 0°C or at 30°C.
911 Aliquots were analyzed by non-reducing SDS PAGE (upper) and BNP (lower), and immunoblotted
912 for Bak to detect linked species. Note that linkage outside the membrane (H164C:H164C') was
913 efficient even at 0°C.

914

915

Figure S4

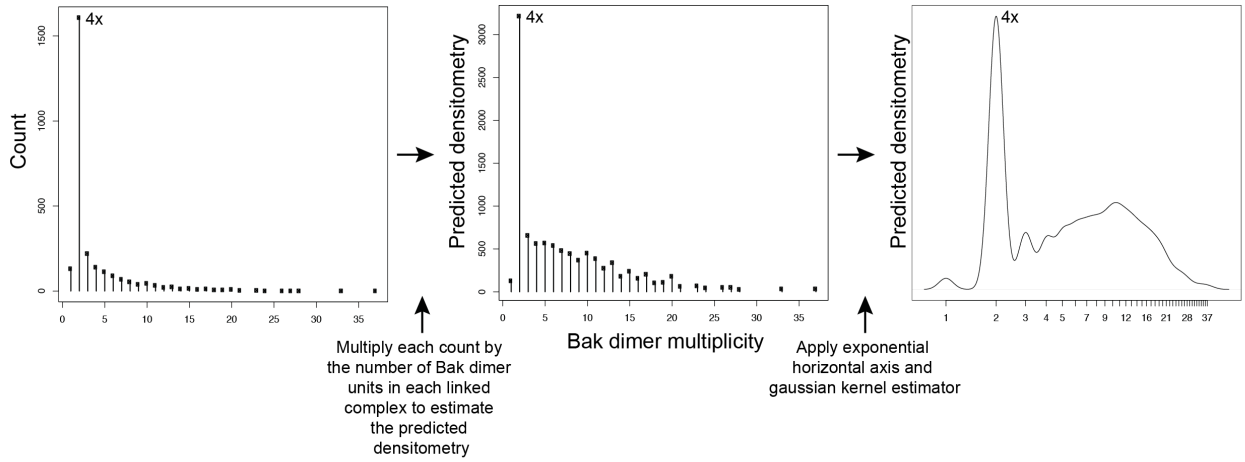

Figure S4 Adjustment to simulation output to allow qualitative comparison to western blot data. Mathematical simulations of Bak dimer linkage generated frequency distributions of the size of Bak complexes (multiples of Bak dimers). These frequency distributions were then transformed to a predicted densitometry by multiplying each count by the number of Bak dimer units present in each linked Bak complex. For instance, the count representing 2x complexes, is multiplied by 1, the count representing 4x complexes is multiplied by 2, the count representing 6x complexes is multiplied by 3, etc. This predicted densitometry approximates the total relative abundance of Bak molecules in each linked Bak complex, which was then transformed with an exponential horizontal axis to mimic the nonlinear spacing of bands, and a gaussian kernel estimator to approximate the smearing of bands (especially at higher molecular weights) to allow qualitative comparison to western blot densitometry outputs.

Figure S5

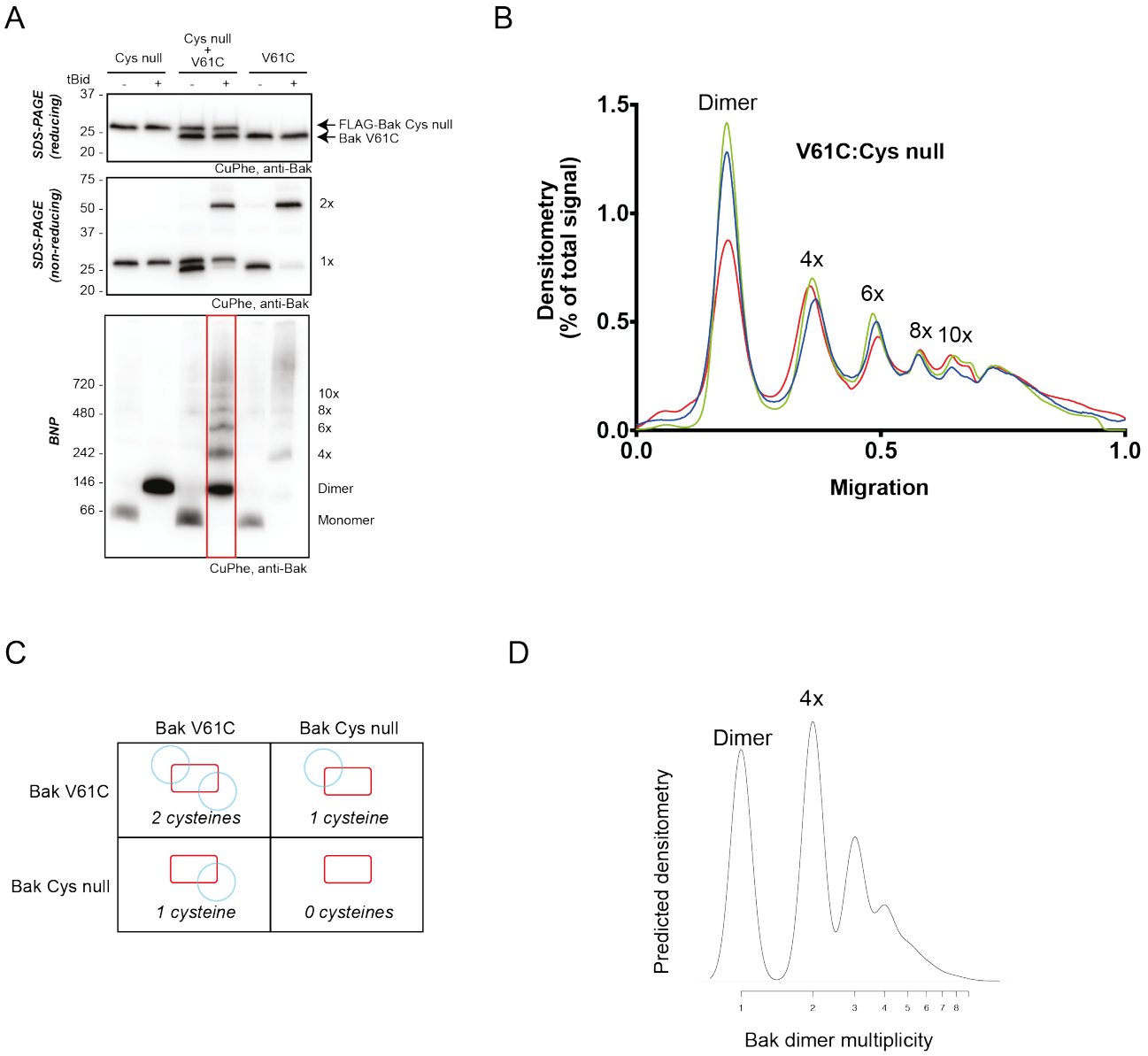

Figure S5 2D simulation with reduced efficiency linkage successfully models reduced linkage in mitochondrial experiments.

(A) Co-expression of Bak V61C with Bak Cys null resulted in less high order linkage species on BNP. Membrane fractions expressing Bak V61C, FLAG-Cys null, or both, were incubated with or without tBid, and then subjected to CuPhe linkage and analysis by BNP, non-reducing SDS PAGE or reducing SDS PAGE.

(B) Densitometry of BNP linkage data following tBid treatment for 3 replicates of the V61C:Flag-Cys null co-expression. Data are normalised to the area under the curve.

(C) Diagram showing the four types of dimers that would form upon co-expression of V61C and Cys null variants of Bak (i.e. a system in which 50 % of Bak molecules are unable to link). Note that dimers will be capable of 0, 1 or 2 linkages.

(D) The 2D simulation was altered to incorporate 50% linkage-incompetent Bak molecules. This simulation yielded a good concordance with the V61C:Flag Cys null densitometry.

Figure S6

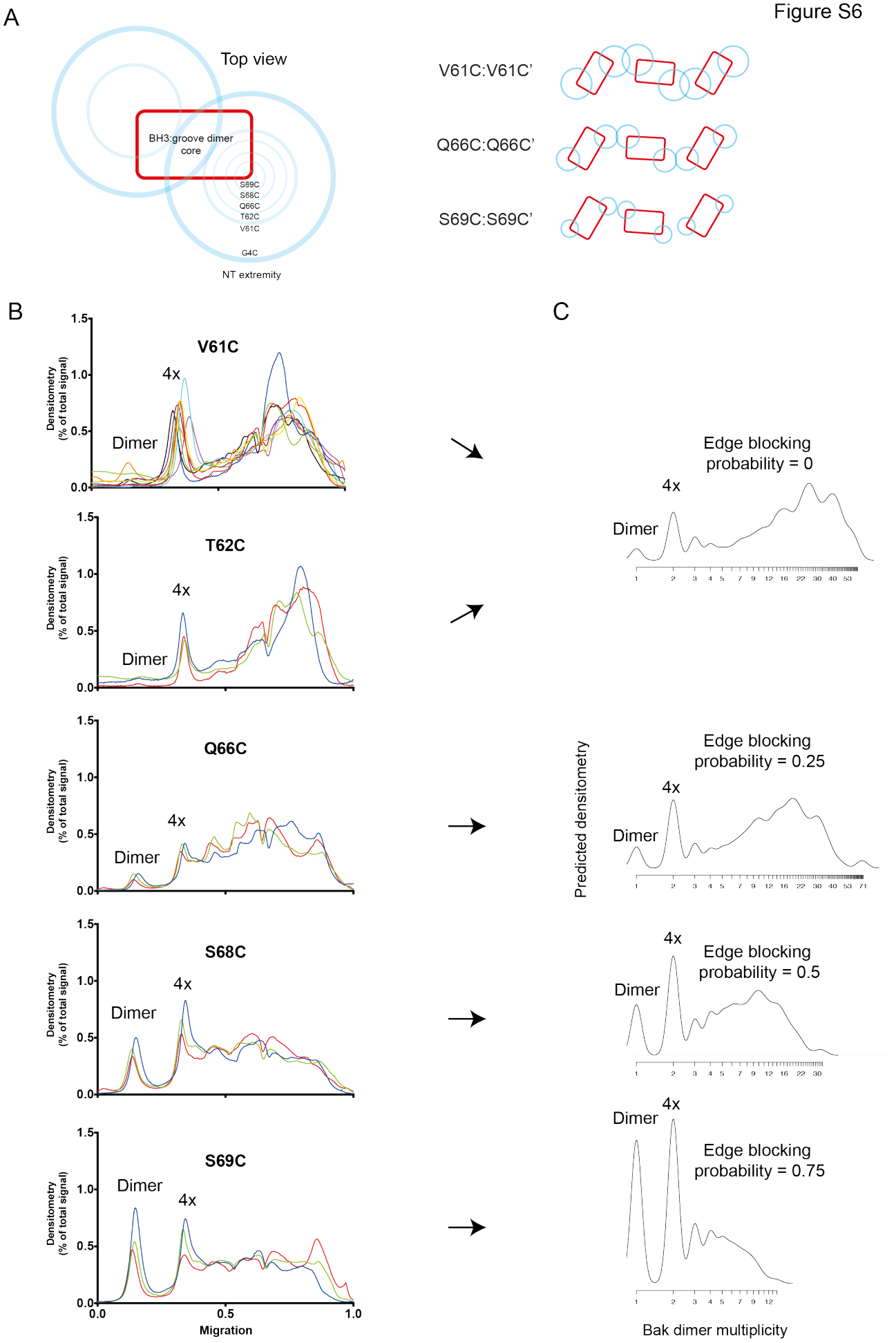

943

Figure S6 2D simulation with edge blocking probability successfully models mitochondrial experiments in which Bak linkage becomes constrained as cysteines are positioned closer to the dimer core.

(A) Residues between V61C and the core of the Bak dimer have a progressively more limited range of movement. On the left, blue circles are shown on a schematic of the Bak dimer to represent the range of movement for G4C, V61C, T62C, Q66C, S68C and S69C. On the right, an illustration of the reduced overlap of Bak dimer extremities (blue circles) is shown for residues with progressively smaller ranges of movement (e.g. V61C>Q66C>S69C).

(B) Densitometry of BNP outputs from V61C, T62C, Q66C, S68C and S69C highlight the reduced linkage efficiency (relative to V61C) as cysteine substitutions approach the constrained core of the Bak dimer.

(C) The 2D simulation was altered to incorporate an "edge blocking probability" to mimic the increasing linkage constraint experienced by cysteine substitutions as they approached the core. The best approximation of each cysteine substitution mutant is indicated by arrows.